PITHA 03/14
IPPP/03/83
FERMILAB-Pub-03/410-T
hep-ph/0401002
December 31, 2003

Effective theory calculation of resonant high-energy scattering

M. Beneke[a], A.P. Chapovsky[a], A. Signer[b] and G. Zanderighi[c]

[a]*Institut für Theoretische Physik E, RWTH Aachen, D–52056 Aachen, Germany*

[b]*IPPP, Department of Physics, University of Durham, Durham DH1 3LE, England*

[c]*Fermi National Accelerator Laboratory, Batavia, IL 60510-500, USA*

Abstract

Tests of the Standard Model and its hypothetical extensions require precise theoretical predictions for processes involving massive, unstable particles. It is well-known that ordinary weak-coupling perturbation theory breaks down due to intermediate singular propagators. Various pragmatic approaches have been developed to deal with this difficulty. In this paper we construct an effective field theory for resonant processes utilizing the hierarchy of scales between the mass of the unstable particle, M, and its width, Γ. The effective theory allows calculations to be systematically arranged into a series in g^2 and Γ/M, and preserves gauge invariance in every step. We demonstrate the applicability of this method by calculating explicitly the inclusive line shape of a scalar resonance in an abelian gauge-Yukawa model at next-to-leading order in Γ/M and the weak couplings. We also discuss the extension to next-to-next-to-leading order and compute an interesting subset of these corrections.

1 Introduction

An important part of recent and future high-energy physics experiments belongs to the detailed investigation of the production of heavy unstable particles, such as W and Z bosons, top quarks, Higgs bosons or perhaps other new particles. From single resonant or pair production the masses and couplings of the particles can be determined with high precision, provided theoretical calculations are equally precise. Since the decay widths of the particles are often non-negligible, this includes a consistent treatment of finite-width effects beyond the narrow-width approximation.

Several higher-order calculations involving unstable particles have been performed in recent years, in particular for the line shape of the Z boson [1], W-pair production [2], and $t\bar{t}$-production [3]. In these calculations the finite width of the particles has been treated in a variety of often pragmatic approaches. While this may be adequate for the present, it is certainly desirable to formulate a theoretical framework that would allow for systematic improvements of the accuracy of such calculations. Moreover, future precision experiments require that such a framework be developed.

The difficulty with unstable particles is that they cause singularities in propagators, if the scattering amplitudes are constructed according to the rules of weak-coupling perturbation theory. A well-known remedy of the singularity is resummation of self-energy corrections to the propagator, which results in the substitution

$$\frac{1}{p^2 - M^2} \;\to\; \frac{1}{p^2 - M^2 - \Pi(p^2)}. \tag{1}$$

The self-energy has an imaginary part of order $M^2 g^2 \sim M\Gamma$, where Γ is the on-shell decay width of the resonance, rendering the propagator large but finite. "Dyson resummation" sums a subset of terms of order $(g^2 M^2/[p^2 - M^2 + iM\Gamma])^n \sim 1$ (near resonance) to all orders in the expansion in the coupling g^2. This procedure raises the question of how to identify all terms (and only these terms) required to achieve a specified accuracy in g^2 and Γ/M. The failure to address this question may lead to a lack of gauge invariance and unitarity of the resummed amplitude, since these properties are guaranteed only order-by-order in perturbation theory, and for the exact amplitude.

Many of the current approaches to unstable particles take the restoration of gauge invariance as their starting point. One example is the fermion-loop scheme [4], which is based on the observation that the dominant contribution to the width of the W and Z gauge bosons comes from fermion loops. The prescription reads to include the fermion-loop corrections in propagators and vertices, so that gauge invariance is maintained, since all fixed-order $g^2 N_f$ terms (where N_f is the number of fermion flavours) are included. Besides the restriction to gauge bosons the disadvantage of this scheme is that one-loop vertices must be computed even for a leading-order approximation. Another scheme [5] constructs a gauge-invariant non-local effective action, which can be matched onto the two-point functions of the underlying theory. The gauge Ward identities are satisfied by construction in this scheme. Both schemes have been implemented in four-fermion production mediated by W-pair production solving not only the gauge-invariance problem but also capturing

some sophisticated features such as running of the couplings. However, it is not evident how to extend them to a systematic approximation of the scattering amplitude in powers of g^2 and Γ/M.

Other approaches exploit the presence of two different momentum scales in the production and decay of weakly interacting unstable particles: M, the mass of the unstable particle, and its width, $\Gamma \ll M$, both related to the location of the resonance pole. In the pole scheme [6] the scattering amplitude is approximated by an expansion in Γ/M around the poles in the complex plane. The coefficients of this expansion must be gauge-invariant in every order. In pair production of unstable particles this approximation is referred to as "double-pole approximation" [2]. It has been used in the complete next-to-leading order (NLO) calculation for W-pair production [2], where in one-loop radiative corrections the leading term in the Γ/M expansion is sufficient.

The pole approximation can be considered as the first step towards a systematic approximation scheme to the scattering amplitude based on the separation of scales. Within the (double) pole approximation the process naturally consists of production and decay subprocesses, connected by the intermediate resonance(s). One-loop corrections separate into two subsets: *factorizable corrections* to the hard production/decay subprocesses, and *non-factorizable corrections*, accounting for interference between different hard subprocesses. This separation does not occur at the level of individual Feynman diagrams. For example, the self-energy correction to the unstable particle contains both, factorizable and non-factorizable pieces, and the two have to be separated carefully to avoid double counting. This is expected to be complicated for multi-loop calculations, or for a calculation of Γ/M suppressed contributions, which lie beyond the pole approximation. One-loop non-factorizable corrections have been extensively studied in the double-pole approximation. A few important theorems have been proved [7], and explicit calculations have been performed [8]. We also mention an approach that constructs the expansion in g^2 of the resonant propagator squared in the distribution sense [9], also addressing the issues of gauge invariance and systematic expansions.

In [10] it was suggested to use the scale hierarchy $\Gamma \ll M$ for constructing an effective field theory, from which hard modes with momenta of order M or larger are removed. The effect of the hard modes is included into the coefficients of the effective Lagrangian and corresponds to the factorizable corrections. Non-factorizable effects are reproduced by the dynamical modes of the effective theory. This provides a more precise definition of "factorizable" and "non-factorizable" that generalizes to higher loop orders. In [10] it was shown that this approach is equivalent to the double-pole approximation within the accuracy of the latter (i.e. one-loop, leading order in Γ/M). However, the idea should work beyond these approximations.

In this paper we pursue this idea and develop the effective field theory approach to unstable particle production from a systematic point of view. We take the attitude that the scale hierarchy $\Gamma \ll M$ is *the* characteristic feature of the process, and that all other issues such as resummation and gauge invariance will be an automatic consequence of any theory that formulates the rules for an expansion in g^2 and Γ/M correctly. We identify the factorization properties of the process to any order in Γ/M, and define the effective

production and decay vertices and the effective Lagrangian in dimensional regularization. The matching corrections are computed by expansion of Feynman integrals in momentum regions [11]. In this way we identify all contributions to the scattering amplitude at a given order in g^2 and Γ/M (and only these). We believe that this approach solves the conceptual difficulties that have so far been associated with the perturbative treatment of unstable particles in principle; however, for complex scattering processes, the implementation in higher orders than NLO still requires difficult calculations.

Here we shall describe our approach for the case of inclusive production of a single charged scalar resonance in fermion-fermion scattering in an abelian gauge model. The specific set-up of the toy model, and the restriction to inclusive scattering, imply that a minimal set of effective fields needs to be introduced, and only the forward scattering amplitude needs to be considered. This allows us to concentrate on the essential features of the approach, such as the identification of momentum modes, factorization of the scattering amplitude, construction of the effective Lagrangian and matching, and the calculation of the scattering amplitude in the effective theory. We compute explicitly the inclusive line shape of the scalar particle in this toy model, and discuss some features at the next-to-next-to-leading order related to gauge invariance and $g^2\Gamma/M$ corrections. The generalization of the method to final states with detected particles or jets, to non-abelian gauge bosons, and to pair production appears not to encounter major new conceptual issues, but requires more technical work, which we hope to complete in the future. A brief exposition of the effective theory approach discussed in the present paper has been given in [12].

The outline of the paper is as follows. In Section 2 we define our toy theory and proceed to discuss in a non-technical manner the ingredients of the effective field theory method: the momentum scales, the presence of soft and collinear modes, the effective interactions and the expression for the forward scattering amplitude in the effective theory. We outline a hierarchy of effective theories, in which collinear fields are either kept or integrated out. The section concludes with a leading-order calculation of the line shape and a discussion of scheme-dependence and matching to the off-resonance cross section. The real virtue of the effective theory approach becomes only apparent when one goes beyond leading order. A complete next-to-leading order calculation is carried out in Section 3, where we compute the two-loop matching of the two-point interaction, and the one-loop matching of the production vertex, required at NLO. The NLO result is completed with the calculation of the forward scattering amplitude in the effective theory. At the end of Section 3 we perform a numerical comparison of the leading-order and next-to-leading-order line shape. The formalism is sufficiently general to allow a systematic extension to next-to-next-to-leading order. While there is no point of doing this calculation in our toy model, we outline the principles of such a calculation in Section 4. Then, as an example of a next-to-next-to-leading order contribution, we compute the one-loop short-distance coefficient of the Γ/M-suppressed production-decay operators and illustrate how a gauge-independent result is obtained automatically from a combination of self-energy, vertex, and box diagrams. We conclude in Section 5. The renormalization constants of the toy theory are collected in an Appendix.

2 Outline of the method

In this section we explain the essential features of our approach. We first set up the toy field theory and scattering process that we consider in this paper. We then discuss the short- and long-distance scales in resonant scattering, the corresponding momentum modes, and derive a representation of the scattering amplitude, in which the different scales are factorized, allowing for an expansion in Γ/M. We end this section by giving the two-to-two forward scattering amplitude at leading order, and obtain from this the leading-order line shape of the resonance.

2.1 Definition of the model

We shall consider the resonant production of a massive scalar particle in the scattering of two massless Dirac fermions. The scalar and one of the fermions (the "electron") are assumed to be charged under an abelian gauge symmetry, the other fermion (the "neutrino") is neutral. The charges are supposed to be equal, so as to allow a scalar-electron-neutrino Yukawa coupling. The theory is much simpler than the electroweak Standard Model, but we find that all conceptual issues related to the treatment of the scalar resonance can be addressed in this toy model.

We thus assume the Lagrangian

$$\begin{aligned}\mathcal{L} &= (D_\mu\phi)^\dagger D^\mu\phi - \hat{M}^2\phi^\dagger\phi + \bar{\psi}i\not{D}\psi + \bar{\chi}i\not{\partial}\chi - \frac{1}{4}F^{\mu\nu}F_{\mu\nu} - \frac{1}{2\xi}\left(\partial_\mu A^\mu\right)^2 \\ &\quad + y\phi\bar{\psi}\chi + y^*\phi^\dagger\bar{\chi}\psi - \frac{\lambda}{4}(\phi^\dagger\phi)^2 + \mathcal{L}_{\rm ct},\end{aligned} \tag{2}$$

where $\mathcal{L}_{\rm ct}$ denotes the counterterm Lagrangian, and the scalar self-interaction is included to make the model renormalizable. Fields and parameters are renormalized in the $\overline{\rm MS}$ scheme. The letter $\hat{M}$ is used to distinguish the $\overline{\rm MS}$ mass (at scale μ) from the pole mass M defined below. Explicit expressions for the counterterm Lagrangian and the renormalization constants are given in the Appendix. The gauge coupling g and Yukawa coupling y are assumed to be of the same order. We define $\alpha_g = g^2/(4\pi)$, $\alpha_y = (yy^*)/(4\pi)$, and use α to refer to them summarily. With no arguments the couplings are evaluated at scale μ. In general, we cannot set the scalar self-coupling λ to zero, but we would like it to be small (for simplicity of the model). Without fine-tuning it is consistent to assume that $\alpha_\lambda/(4\pi) \equiv \lambda/(16\pi^2)$ is of order $\alpha^2/(4\pi)^2$, since the leading counterterm is of this order. We shall assume this counting in the following.

We shall consider the totally inclusive cross section in electron-neutrino scattering,

$$\bar{\nu}(q) + e^-(p) \to X, \tag{3}$$

as a function of the center-of-mass energy squared $s = (q+p)^2$ in the vicinity of $s \approx M^2$, where we expect an enhancement of the cross section due to the resonant production of the charged scalar. By vicinity we mean that $s - M^2 \sim M\Gamma \sim M^2\alpha \ll M^2$. Because the

electron is massless, the total cross section is not infrared-safe. The initial-state collinear singularity should be factorized into the electron distribution function. This being understood, we will usually quote the "partonic" cross section with the singularity regularized in dimensional regularization and subtracted minimally. Note that strictly speaking the electron distribution function is not defined if the electron is truly massless as assumed in (2); however, we may always assume that the electron has a mass much smaller than any other scale in the scattering process. We can then neglect the mass in the Lagrangian, keeping in mind that it must be reintroduced to regularize the distribution function.

Our aim is to approximate this totally inclusive line shape of the scalar resonance in electron-neutrino scattering systematically in powers of g^2 and

$$\delta \equiv \frac{s - \hat{M}^2}{\hat{M}^2} \sim \frac{\Gamma}{M}. \tag{4}$$

This cannot be done with standard methods, since there are kinematic enhancements proportional to $\alpha\hat{M}^2/(s - \hat{M}^2) \sim 1$ at every order in the perturbation expansion in α. This is the origin of the well-known need for resummation.

2.2 Effective Lagrangians, effective vertices and representation of the scattering amplitude

In space-time the resonance is produced in the collision with a characteristic formation time of order $1/M$, lives a much longer time of order $1/\Gamma$, and then decays, again within a short time of order $1/M$. We therefore expect some kind of factorization between production, propagation and decay. This essentially classical space-time picture is corrected, because quantum fluctuations exist at all scales. Factorization persists quantum-mechanically, since only long-wavelength fluctuations can resolve the details of production and decay (separated by the long time interval $1/\Gamma$) simultaneously. The resulting picture is shown in the left-hand graph of Figure 1 below. (The right-hand graph shows the featureless "background processes", in which the final state of the collision is produced without the resonance.) Factorization in the presence of quantum corrections can be implemented with the effective Lagrangian technique.

2.2.1 Effective Lagrangian for soft and collinear interactions

To obtain the expansion of the line-shape in δ, we construct the effective Lagrangian and effective vertices for the long-distance contributions to the process. "Hard" effects related to quantum fluctuations with momenta $k \sim M$ are included as coefficient functions by matching the effective Lagrangian to the underlying theory. This can be done in ordinary weak-coupling perturbation theory, since hard propagators, being off-shell by an amount of order M^2, do not cause kinematic enhancements proportional to $1/\delta$. Each Feynman diagram is broken into a hard and other contributions similar to the non-relativistic expansion of Feynman integrals [11]. The hard region corresponds to the Taylor expansion of the Feynman *integrand* in δ (counting the loop momentum $k \sim M$), and goes into

the coefficient functions of the effective Lagrangian and effective vertices. The remaining regions correspond to momentum configurations, where propagators are near mass-shell. They must be reproduced by the diagrams in the effective theory.

What are the momentum modes in the effective theory? Parameterize the momentum of the scalar particle near resonance by $P = \hat{M}v + k$, where the velocity vector $v^2 = 1$ and the residual momentum k scales as $M\delta \sim \Gamma$. Then $P^2 - \hat{M}^2$ remains small, of order $M\delta$, if the scalar interacts with a "soft" fluctuation with momentum of order $M\delta$. The effective theory therefore contains soft massless modes, and the heavy scalar near mass-shell. (To emphasize the fact that the form of the effective theory is very much the same for stable and unstable particles, we will also call the heavy scalar near mass-shell a "soft" mode. In previous work [10] the term "resonant mode" has been used.) Note that soft interactions do not change the velocity vector of the scalar. We therefore define a field $\phi_v(x)$ with the rapid spatial variation $e^{-i\hat{M}v\cdot x}$ removed to represent the heavy scalar with momentum near $\hat{M}v$. The field $\phi_v(x)$ carries only the residual slow variation in x over distances of order $1/\delta$. If the heavy particle was a stable heavy quark, the effective Lagrangian that describes its interactions with soft quark and gluon fluctuations would be the heavy quark effective Lagrangian [13], which has become a standard tool in heavy quark physics to separate the physics on the scales M and $\Lambda_{\rm QCD}$. The corresponding Lagrangian for an unstable scalar is

$$\mathcal{L}_{\rm HSET} = 2\hat{M}\,\phi_v^\dagger \left(iv\cdot D_s - \frac{\Delta}{2} \right) \phi_v - \frac{1}{4}\,F_{s\mu\nu}F_s^{\mu\nu} + \bar{\psi}_s i\not{D}_s \psi_s + \bar{\chi}_s i\not{\partial}\chi_s + \ldots . \qquad (5)$$

Here $D_s = \partial - igA_s$ denotes the covariant derivative with a soft photon field, and we have kept the relativistic normalization with mass dimension 1 for the non-relativistic scalar field ϕ_v, hence the factor $2\hat{M}$. Furthermore, ψ_s (χ_s) stands for the soft electron (neutrino) field. Only the leading power in the expansion in $1/\hat{M}$ has been given, but there is no difficulty in adding further terms. The leading-power Lagrangian contains a single short-distance matching coefficient, Δ, which can be related to the resonance pole position $M^2 - iM\Gamma$ as we discuss below (Section 3.1). In the pole renormalization scheme Δ equals $-i\,\Gamma$. Since the Lagrangian describes only effects related to the soft scale $M\delta$, all dimensionful quantities can be assigned a scaling power of δ. (In such assignments, we set $M = 1$. Dimension is restored by inserting the appropriate power of M.) Partial derivatives and the soft photon field count as δ. The field ϕ_v as well as soft massless fermion fields count as $\delta^{3/2}$, because their position-space propagator is proportional to $1/x^3 \sim \delta^3$. In particular, since Δ is of order $\Gamma \sim M\alpha \sim \delta$, and so is $iv\cdot D_s$, the decay width of the heavy scalar, or, more generally, the coefficient Δ, is a leading-power effect in the Lagrangian, and must be included in the scalar propagator. This is the effective theory counterpart of the familiar self-energy resummation.

The effective theory is not yet complete, because the scalar is produced in the scattering of energetic ($E \sim M$) massless particles. To describe these "collinear" modes, we suppose that the electron moves with large momentum in the direction of $\vec{n}_-$, and introduce two reference light-like vectors, $n_\pm$, with $n_+^2 = n_-^2 = 0$ and $n_+n_- = 2$. A collinear momentum

is decomposed as

$$p^\mu = (n_+p)\,\frac{n_-^\mu}{2} + p_\perp^\mu + (n_-p)\frac{n_+^\mu}{2}, \tag{6}$$

where $n_+p \sim M$, $n_-p \sim M\delta$ and $p_\perp \sim M\delta^{1/2}$. The scaling of the small components is determined by the interaction of collinear modes with soft modes, which implies that a generic collinear fluctuation has an off-shellness of order $\hat{M}\delta$. The scaling of the transverse component is then fixed by the poles of collinear propagators. Collinear modes in an effective field theory framework have been discussed previously in B meson decays into light energetic mesons [14]. Our set-up is in fact very similar to this case, since the production of the scalar resonance represents the "inverse" kinematics of B decay. The neutrino plays the role of the weak current, so that we consider the production of a heavy particle by scattering an energetic electron on this "current". The effective Lagrangian for the interactions of collinear modes and soft modes is, again at leading power in the expansion in δ,

$$\mathcal{L}_{\rm SCET} = \bar\psi_c \left(in_-D + i\not{D}_{\perp c} \frac{1}{in_+D_c + i\epsilon}\, i\not{D}_{\perp c} \right) \frac{\not{n}_+}{2}\,\psi_c - \frac{1}{4}\,F_{c\mu\nu}F_c^{\mu\nu} + \ldots, \tag{7}$$

where ψ_c denotes the collinear electron field, which satisfies $\not{n}_-\psi_c = 0$ [15, 16]. The covariant derivative $iD_c = i\partial + gA_c$ contains the collinear photon field. The interaction with the soft field appears only in $in_-D = in_-\partial + gn_-A_c + gn_-A_s$. Again there is no difficulty in going to higher orders in the expansion; we discuss this below (Section 3.2). The δ power counting is as follows: the components of derivatives on collinear fields and the collinear photon field scale as the corresponding collinear momentum components; the collinear fermion field scales as $\psi_c \sim \delta^{1/2}$ as seen from the propagator. Note that there do not exist collinear interactions with the heavy scalar in the Lagrangian, since the coupling of a collinear mode to the on-shell scalar causes the scalar propagator to become hard. These hard effects are already integrated out, and appear as effective production and decay vertices (see the following subsection). Finally, we must add an effective Lagrangian for the collinear neutrino field. Adopting a frame where the electron and neutrino collide head-on, the neutrino Lagrangian is obtained from (7) by substituting $\psi_c \to \chi_{c2}$, interchanging $n_- \leftrightarrow n_+$, and replacing all covariant derivatives by ordinary derivatives. At the level of the leading Lagrangian the neutrino is non-interacting.

To summarize, Feynman diagrams in resonant scattering involve contributions from the following three momentum regions:

$$\begin{aligned} \text{hard (h):} &\qquad p \sim M \\ \text{soft (s):} &\qquad p \sim M\delta \\ \text{collinear (c1):} &\qquad p_\perp \sim M\delta^{1/2},\; n_+p \sim M,\; n_-p \sim M\delta \end{aligned} \tag{8}$$

(We note that what we call "soft" here is called "ultrasoft" in [16] and much of the literature on soft-collinear effective theory.) In the general case several types of collinear modes are required, one for each direction defined by energetic particles in the initial and final state. For the inclusive line shape we calculate the forward scattering amplitude, so no direction

is distinguished in the final state. We then need two sets of collinear modes, one for the direction of the incoming electron, labeled by "c1" (or often simply "c"), the other for the direction of the incoming neutrino (labeled "c2"). When the hard fluctuations are integrated out, the effective Lagrangian is built from the soft heavy scalar ϕ_v, a soft and collinear photon, A_s and A_{c1}, respectively, a collinear and a soft electron, ψ_{c1} and ψ_s, and a c2-collinear and soft neutrino, χ_{c2} and χ_s. (In complete generality, we should also introduce the collinear fields ψ_{c2}, A_{c2} and χ_{c1}, but they appear only in highly suppressed terms, so we can ignore them here.) The effective interactions of these modes are described by the sum of $\mathcal{L}_{\rm HSET}$ and the soft-collinear effective Lagrangians for the two directions. In order to describe resonant scattering with a desired accuracy one has to match the Lagrangian to this accuracy, and calculate the scattering amplitude in the effective theory. The relevant terms can be identified a priori by applying the δ power counting rules.

2.2.2 Effective vertices

The effective Lagrangian misses an essential piece of physics. Since $\mathcal{L}_{\rm HSET}$ does not contain collinear fields, and since $\mathcal{L}_{\rm SCET}$ does not contain the heavy scalar field, the two can interact only through soft modes. In particular, there is no vertex in the Lagrangian that allows the production of the scalar in the scattering of energetic particles.

Such vertices cannot be included in the effective Lagrangian for soft and collinear terms as interaction terms, because they contribute to the scattering matrix element in the effective theory only in a very specific pattern. For instance, a vertex with fields $\phi_v\bar{\psi}_{c1}\chi_{c2}$ can occur exactly twice, once for the production of the scalar, and once for its decay. Multiple insertions are not compatible with the kinematic restrictions on the process, which allow only one nearly on-shell scalar line in any diagram by energy conservation. Note that a diagram in the full theory may of course have many internal scalar lines. However, these will generally be far off-shell ("hard") and these hard effects are included in the coefficient functions of the Lagrangian and effective vertices. What we are discussing here is the structure of possible diagrams/scattering processes after hard effects are integrated out.

In more technical terms the interaction of two collinear modes with opposite directions, here the electron and the neutrino, produces a hard momentum configuration with invariant mass squared *of order* M^2, and therefore cannot be included in the effective Lagrangian. What we actually need is that the momenta of the oppositely moving collinear modes are pre-arranged (by the experimenter who sets up the beam energy to be near resonance) to produce a configuration with invariant mass squared *equal* to M^2 within a small amount of order $M^2\delta \sim s - M^2$. To account for these configurations we introduce production and decay vertices ("effective vertices"). The leading-order vertex is simply the original Yukawa coupling expressed in terms of the fields in the effective theory,

$$J(x) = e^{-i\hat{M}v\cdot x}\, y\,[\phi_v\bar{\psi}_{c1}\chi_{c2}](x). \tag{9}$$

In higher order in α or δ a larger set of operators – not necessarily local – is generated by integrating out hard quantum fluctuations and the coefficient function will receive correc-

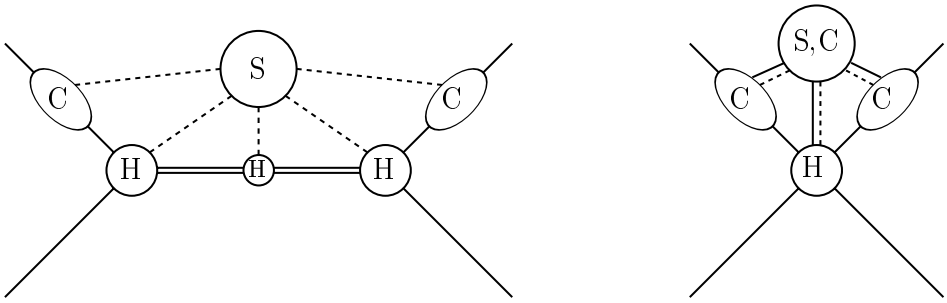

Figure 1: Reduced diagram topologies in $2 \to 2$ scattering near resonance. Left: resonant scattering. Right: non-resonant scattering. See text for explanations.

tions. (This will be seen in more detail in Section 3.3.) However, these operators have in common that they contain the field ϕ_v exactly once.

The scattering may also occur without the production of the scalar near its mass-shell. In our toy theory this still requires an intermediate scalar line, since the neutrino has only Yukawa interactions. The scalar may be off-shell, because the electron has radiated an energetic (hard or collinear) photon before it hits the neutrino. In this case the invariant mass of the colliding electron-neutrino system is of order M^2 but not near M^2, producing a non-resonant scalar. In the effective theory this process is represented by production-decay operators, which do not contain ϕ_v fields. The simplest operator of this type has the coupling and field structure

$$T(x) \sim |y|^2 \, [(\bar{\psi}_{c1}\chi_{c2})(\bar{\chi}_{c2}\psi_{c1})](x). \tag{10}$$

In general, non-resonant scattering includes all "background processes", which produce one of the final states under consideration.

With these preparations we obtain the following formula for the forward $2 \to 2$ scattering amplitude in the effective theory:

$$i\,\mathcal{T} = \sum_{m,n} \langle \bar{\nu}e| \int d^4x \, T\{iJ_m^\dagger(0) iJ_n(x)\} |\bar{\nu}e\rangle + \sum_k \langle \bar{\nu}e| iT_k(0) |\bar{\nu}e\rangle, \tag{11}$$

where in the first term "T" denotes time-ordering, and where the sums extend over the sets of effective vertices of the two types, J or T. The matrix elements on the right-hand side are evaluated with the effective Lagrangian for soft and collinear fields. This result is depicted in graphical form in Figure 1. The "resonant" scattering term on the left-hand side involves a production and decay vertex, and collinear interactions at the electron legs, which connect to the production and decay vertex. Soft (and only these) fields can connect to all parts of the diagram. The double line denotes the heavy resonance, solid lines collinear modes and dashed lines soft modes. A single solid (dashed) line may represent a collection of several collinear (soft) fields, depending on the structure of the effective interaction. Collinear fields cannot be exchanged from the left to the right of a resonant

diagram, since this would cause the scalar to be off-shell. The corresponding configurations are included in the "non-resonant" scattering topology on the right-hand side of the figure. This topology does not involve a resonant heavy scalar, and both soft and collinear fields can be exchanged across the diagram.

The various terms in (11) can be ordered according to their scaling with δ and α, thus allowing for a determination of the terms needed for a calculation to some accuracy before performing any computation. We will now estimate the importance of the resonant and non-resonant contributions by a simple power counting argument, taking as representatives the leading interactions of each type. Combining the scaling of the fields we find $J \sim y\,\delta^{5/2}$ from (9). Furthermore x is soft, since x represents the distance of order $1/\delta$ over which the resonant scalar propagates, hence d^4x in (11) counts $1/\delta^4$. The normalization of states implies that an external collinear particle counts as $1/\delta^{1/2}$, so $|\bar{\nu}e\rangle \sim 1/\delta$. Putting everything together, we obtain

$$\sigma \sim \frac{1}{s}\,\mathrm{Im}\,\mathcal{T} \sim \frac{|y|^2}{\delta} \sim \frac{|y|^2}{M\Gamma}, \tag{12}$$

which is the expected result. The leading non-resonant scattering operator T in (10) scales as $|y|^2\,\delta^2$. The matrix element $\langle\bar{\nu}e|iT(0)|\bar{\nu}e\rangle$ is non-vanishing only at order g^2, since the overlap of T with the external states requires the emission of an energetic photon. Adding the counting of the states, we find that the contribution to $\mathcal{T}$ is of order $g^2|y^2|$. This is suppressed by a factor $g^2\Gamma/M$ relative to (12), hence establishing that non-resonant topologies contribute only at next-to-next-to-leading order in the combined expansion in α and δ. We shall discuss these effects in some detail in Section 4.2.

In this discussion of the non-resonant contribution we assumed that the $(\bar{\psi}_{c1}\chi_{c2})$ operator in T describes an electron-neutrino configuration with invariant mass far from M^2. We shall see below that the applications of the equation of motion to bring the scalar effective Lagrangian into its canonical form generate a local four-fermion operator identical to T, but with $(\bar{\psi}_{c1}\chi_{c2})$ describing an electron-neutrino configuration with invariant mass near M^2. This arises because the resonant propagator is canceled by the rearrangements implied by the equation of motion. In this case T has a non-vanishing tree-level matrix element and contributes already at next-to-leading order.

2.2.3 Soft and collinear fluctuations of collinear modes

The complication mentioned in the previous paragraph, as well as the complication of excluding "by hand" collinear loop contributions to the matrix element of $T\left\{J^\dagger(0)J(x)\right\}$, which connect the initial and final state, can be avoided, if we distinguish modes that differ from the external collinear momenta only by a soft momentum from those which differ by a collinear momentum. Both modes have virtuality $M\delta^{1/2}$ and have been called "collinear" up to now. However, the former can be assigned momentum $\hat{M}n_-/2 + k$, where k is soft and the large collinear component $\hat{M}n_-/2$ is *fixed*. Only the latter represent collinear fluctuations associated with collinear loop momenta.

Just as for the heavy scalar with momentum close to $\hat{M}v$, it is useful to extract the fixed large momentum from the field, and to define

$$\psi_{n_-}(x) = e^{i\hat{M}/2\,(n-x)}\,\mathcal{P}_+\psi_{c1}(x) \tag{13}$$

for soft fluctuations around the external momentum. ($\mathcal{P}_+$ projects on the positive frequency part of ψ_{c1}.) The new field $\psi_{n_-}(x)$ has only variations over distances of order $1/\delta$. For the collinear fluctuations we keep the field $\psi_{c1}(x)$. Similarly we define the field $\chi_{n_+}(x)$.

The collinear effective Lagrangian now assumes a more complicated expression, since we distinguish the interactions of the two types of collinear fields. However, it is now possible to add the effective vertices as interaction terms in the Lagrangian, since the kinematic distinction of configurations with virtualities of order and near M^2 is implemented at the level of the fields. In particular, the effective vertex operator $J(x)$ is now given by

$$y\,[\phi_v\bar{\psi}_{n_-}\chi_{n_+}](x), \tag{14}$$

but there is no interaction vertex of this form with $\bar{\psi}_{n_-}$ replaced by $\bar{\psi}_{c1}$. For the four-fermion operators, we must distinguish $(\bar{\psi}_{c1}\chi_{n_+})(\bar{\chi}_{n_+}\psi_{c1})$ from $(\bar{\psi}_{n_-}\chi_{n_+})(\bar{\chi}_{n_+}\psi_{n_-})$. Since the external collinear state can be created or destroyed only by the softly fluctuating collinear fields and their conjugates, the latter operator has a tree-level matrix element, but the former does not, because it requires interaction vertices of the type $\bar{\psi}_{n_-}\psi_{c1}A_{c1}$ from the collinear Lagrangian to generate a non-vanishing overlap with the external state.

2.2.4 Integrating out collinear fluctuations

The formalism developed up to this point contains propagating soft and collinear modes in the effective theory. We can go one step further and integrate out collinear *fluctuations*, that is we integrate out loops with momenta that scale as collinear momenta. This can be done perturbatively as long as the couplings at the scale $M\delta^{1/2}$ are small. We now sketch the structure of the resultant effective theory. At the level of the calculations in the remainder of the paper there is in fact no difference between the two descriptions before and after integrating out collinear loops, since the collinear loop integrals we encounter all vanish in dimensional regularization.

Technically we introduce two distinct collinear fields as described above and eliminate the fields that describe collinear fluctuations from the effective Lagrangian. With only soft modes remaining in the effective theory, the effective Lagrangian is constructed from the soft electron and photon field, and the fields ϕ_v, ψ_{n_-}, and χ_{n_+}, all scaling as $\delta^{3/2}$. The scattering amplitude can be computed from

$$\mathcal{L} = \mathcal{L}_{\rm HSET} + \mathcal{L}_- + \mathcal{L}_+ + \mathcal{L}_{\rm int}, \tag{15}$$

where $\mathcal{L}_{\rm HSET}$ describes the soft interactions of the heavy scalar as before, and $\mathcal{L}_-$, $\mathcal{L}_+$ are bilinear in the fields $\psi_{n_-}(x)$ and $\chi_{n_+}(x)$, respectively. The soft-collinear Lagrangian $\mathcal{L}_{\rm SCET}$ is non-local due to the presence of $1/(in_+\partial)$, but these non-localities disappear,

when collinear fluctuations are integrated out, and the large component of the energetic fields is "frozen" to $\hat{M}/2$ (modulo soft variations). For instance, consider the leading-power SCET Lagrangian (7) for the electron field, which matches at tree level to the expression

$$\bar{\psi}_{n_-}\left(in_-D_s+\frac{[i\partial_\perp]^2}{\hat{M}}\right)\frac{\not{n}_+}{2}\,\psi_{n_-} \tag{16}$$

in the new effective theory. The term with the transverse derivative squared is already suppressed by one factor of δ compared to the leading term, since derivatives on $\psi_{n_-}(x)$ count as δ. When collinear quantum fluctuations are included, the set of allowed operators consists of operators non-local in $1/(in_-\partial)$, since the n_- component of the external soft momenta of a collinear loop are of the same order as the n_- component of the collinear momentum. These new non-localities, appearing at higher orders in α, correspond to the convolution of a "jet factor" with the remaining soft matrix element. Similar considerations apply to the neutrino field. The fields for the soft fluctuations of the energetic particles now behave in many ways similar to the field for a static heavy particle. In both cases the virtuality is $\hat{M}^2\delta$, and the interaction with soft modes (of virtuality $\hat{M}^2\delta^2$) kicks the particle off its classical trajectory only by a negligible amount; hence the fixed vector that labels the field. (The discussion here is reminiscent of "large-energy effective theory" [17], except that we have in mind a situation where hard *and collinear* modes are eliminated.)

As mentioned above, the production and decay vertices can be implemented as interaction terms $\mathcal{L}_{\rm int}$ in the Lagrangian, because the kinematic restriction that prevented us from adding generic interactions of collinear modes with different directions to the Lagrangian is now implemented at the level of the fields: by construction the scattering of the electron described by $\psi_{n_-}(x)$ and the neutrino described by $\chi_{n_+}(x)$ produces a mode with momentum $\hat{M}v+k$ with k soft. The most general terms allowed for a $2\to 2$ scattering process are of the form $\phi_v\bar{\psi}_{n_-}\chi_{n_+}$ (or its hermitian conjugate) or $(\bar{\psi}_{n_-}\chi_{n_+})\,(\bar{\chi}_{n_+}\psi_{n_-})$ plus additional soft fields. Since none of the fields ϕ_v, ψ_{n_-}, and χ_{n_+} is created or destroyed by the other terms in the Lagrangian, the terms in $\mathcal{L}_{\rm int}$ can only contribute in a topology that corresponds to a classical scattering process of the energetic particles and the heavy scalar. (In particular closed loops of only ϕ_v, ψ_{n_-} and χ_{n_+} lines vanish due to the structure of the poles of the propagators.) These are the two topologies shown in Figure 1 but with the collinear subgraphs eliminated and interpreted as parts of the production and decay vertices. The power counting goes as follows: since $\int d^4x\phi_v\bar{\psi}_{n_-}\chi_{n_+}\sim\delta^{1/2}$, each insertion of this interaction vertex gives a factor of $\delta^{1/2}$. (Even though the effective theory contains only a single scale, we must count powers of δ rather than dimensions due to our unconventional $2\hat{M}$ normalization of the non-relativistic scalar kinetic term.) The insertion of a four-fermion operator carries a δ^2 suppression factor, which results in a δ suppression relative to the resonant contribution, not counting factors of coupling constants.

2.3 Leading-order line shape

We now perform the (trivial) leading-order calculation of the inclusive line shape of the resonance. From the foregoing it follows that we need only the leading-order Lagrangian (5)

together with the leading vertex J in (9). The calculation consists of two steps: matching the effective Lagrangian to the "full" theory to leading order, and the calculation of the forward scattering amplitude in the effective theory. At the end, we use the optical theorem to obtain the line shape.

2.3.1 Matching

Since $iv\partial$ is of order δ on soft fields, we see from (5) that we need Δ to order $\delta \sim \alpha$. This implies that Δ must be chosen so as to reproduce the (renormalized) full theory propagator $i/(p^2 - \hat{M}^2 - \Pi(p^2))$ near the resonance pole with this accuracy. We discuss the matching condition in more technical terms in Section 3.1. At leading order, one finds $\Delta^{(1)} = \Pi^{(1)}(\hat{M}^2)/\hat{M}$, where $\Pi^{(1)}(\hat{M}^2)$ is the renormalized one-loop self-energy evaluated at $p^2 = \hat{M}^2$.

All calculations will be done with dimensional regularization with $d = 4 - 2\epsilon$, where the loop integration measure is defined as

$$[dl] = \left(\frac{\mu^2 e^{\gamma_E}}{4\pi}\right)^{\epsilon} \frac{d^d l}{(2\pi)^d}. \tag{17}$$

With this convention the $\overline{\rm MS}$ scheme corresponds to subtracting all poles in ϵ minimally. In our toy model a straightforward computation of four diagrams

$-i\,\Pi^{(1)} =$ 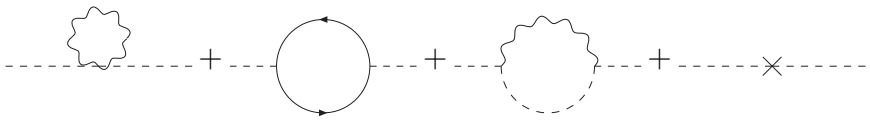 (18)

gives

$$\frac{\Delta^{(1)}_{\overline{\rm MS}}}{\hat{M}} = \frac{\alpha_y}{4\pi}\left(2\ln\frac{\hat{M}^2}{\mu^2} - 4 - 2i\pi\right) + \frac{\alpha_g}{4\pi}\left(-3\ln\frac{\hat{M}^2}{\mu^2} + 7\right) \tag{19}$$

in the $\overline{\rm MS}$ scheme. (Note that the one-loop diagram proportional to the scalar self-coupling λ counts as α^2 and therefore does not contribute to $\Pi^{(1)}$.)

The renormalization scheme dependence of Δ is related to the mass renormalization convention in the underlying theory, if we choose the parameter $\hat{M}$ in the effective theory to be the renormalized mass of the full theory. The effective theory formalism does not rely on a specific renormalization convention. We will use the $\overline{\rm MS}$ convention and the pole mass convention to illustrate this point. The pole mass M is defined through the location of the singularity,

$$\bar{s} = M^2 - iM\Gamma \tag{20}$$

in the scalar propagator. Writing $M = \hat{M} + \delta\hat{M}$, and using $\Delta^{(1)} = \Pi^{(1)}(\hat{M}^2)/\hat{M}$, the relations

$$\delta\hat{M}^{(1)} = \frac{1}{2}\,{\rm Re}\,\Delta^{(1)}, \qquad \Gamma^{(1)} = -{\rm Im}\,\Delta^{(1)} \tag{21}$$

hold at the one-loop order. Note that $\hat{M} = \hat{M}(\mu)$, but we do not indicate the scale-dependence explicitly.

2.3.2 Forward scattering amplitude

The forward scattering amplitude is given at leading order in the effective theory (not distinguishing explicitly between collinear and soft fluctuations of the collinear fields) by

$$\begin{aligned} i\,\mathcal{T}^{(0)} &= \int d^4x\, e^{-i\hat{M}v\cdot x}\,\langle\bar{\nu}e|T\{iy^*\,[\phi_v^\dagger\bar{\chi}_{c2}\psi_{c1}](0)\,iy[\phi_v\bar{\psi}_{c1}\chi_{c2}](x)\}|\bar{\nu}e\rangle_{\rm LO} \\ &= \quad = i^2yy^*\,[\bar{u}(p)v(q)]\,\frac{i}{2\hat{M}(v\cdot k-\Delta^{(1)}/2)}\,[\bar{v}(q)u(p)], \end{aligned} \tag{22}$$

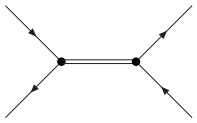

where the double line denotes the resonant propagator defined by the effective Lagrangian $\mathcal{L}_{\rm HSET}$, and $k = p + q - \hat{M}v$. We take $v = (1,\vec{0})$ and the external momenta $p = \sqrt{s}/2\,(1,0,0,-1) = \sqrt{s}/2\,n_-$, $q = \sqrt{s}/2\,(1,0,0,1) = \sqrt{s}/2\,n_+$, so $v\cdot k = \sqrt{s} - \hat{M}$. Note that by construction the effective propagator includes the geometric series of all one-loop self-energy insertions, evaluated at threshold according to the definition of $\Delta^{(1)}$. Performing the polarization average the forward scattering amplitude reads

$$\mathcal{T}^{(0)} = -\frac{yy^*\,s}{4\hat{M}(\sqrt{s}-\hat{M}-\Delta^{(1)}/2)}. \tag{23}$$

Note that because we used spinors $u(p)$ etc. for the external states, $\mathcal{T}^{(0)}$ contains next-to-leading order terms from the factor $s = \hat{M}^2 + [s-\hat{M}^2]$ in the numerator. For a strict expansion it would be more appropriate to use the spinors $u(\hat{M}n_-/2)$ etc., in which case $\mathcal{T}^{(0)}$ would be strictly leading order, but in practice it may be convenient not to perform this trivial expansion in order to reduce the number of terms.

2.3.3 Inclusive line shape

The inclusive line shape is related to the forward scattering amplitude by the optical theorem, which gives

$$\begin{aligned} \sigma^{(0)} &= \frac{1}{s}\,\mathrm{Im}\,\mathcal{T}^{(0)} = \frac{yy^*}{4\hat{M}}\,\frac{\Gamma^{(1)}/2}{(\sqrt{s}-[\hat{M}+\delta\hat{M}^{(1)}])^2+{\Gamma^{(1)}}^2/4} \\ &= \frac{\pi\alpha_y^2}{4}\,\frac{1}{(\sqrt{s}-[\hat{M}+\delta\hat{M}^{(1)}])^2+(\alpha_y\hat{M}/4)^2}, \end{aligned} \tag{24}$$

where we used (21). The line shape has the form of a Breit-Wigner distribution in the center-of-mass energy $\sqrt{s}$. This is in fact the universal line shape that appears in the leading-order approximation to any resonant $\bar{\nu}e$ scattering process in our toy model, but the line shapes will depend on the final state beyond this approximation. (It is a matter of convention whether we divide by s to obtain the cross section from the forward scattering amplitude, or expand this factor around $\hat{M}^2$. Here we keep $1/s$ unexpanded, so that the factor of s in the numerator of (23) is canceled, and the leading-order line shape assumes an exact Breit-Wigner distribution.)

In the presence of fields for unstable particles unitarity and the optical theorem apply to the scattering matrix defined on the Hilbert space of stable particle in- and out-states only, since the resonance does not correspond to an asymptotic particle state [18]. The optical theorem can be interpreted as taking the sum over all "cuts" of a diagram, where now the line for the unstable particle propagator must not be cut. For the leading order diagram in (22) this means that cutting the effective propagator represents the sum over all possible cuts of the one-loop self-energy insertions implicitly contained in the double-line propagator. This corresponds to cutting the second diagram in (18), which is responsible for the leading-order decay width $\Gamma^{(1)}$ of the scalar.

We remark that the effective Lagrangian is not real, since the hard coefficient functions have imaginary parts, but this does not lead to a non-unitary time evolution. Consider, for instance, the diagram in (22). Unitarity requires an amplitude that corresponds to the "square" of this diagram, but the effective theory does not contain diagrams with closed electron-neutrino loops. Rather the corresponding (short-distance) effect is included in the complex coefficient function. Matching the effective theory to the underlying theory automatically guarantees that the combination of effective theory diagrams and complex couplings reproduces the unitary time-evolution to the desired accuracy.

The calculation shows that if the result is represented in two different mass renormalization schemes, the masses must be related to one-loop accuracy for a consistent change of conventions. For instance, if the pole mass $M = 100\,\mathrm{GeV}$ is known from elsewhere, the $\overline{\mathrm{MS}}$ mass for $\mu = \hat{M}$ is $\hat{M} = M - \delta\hat{M}^{(1)} = 98.8\,\mathrm{GeV}$, where we use $\alpha_y = \alpha_g = 0.1$ to illustrate the numerics. From (24) we see that the denominator contains $\sqrt{s} - M$ in *any* scheme to one-loop accuracy, but there is a residual scheme dependence (and scale dependence, since $\hat{M}$ depends on μ) due to the width $\alpha_y\hat{M}/2$. This is a NLO effect, which will be reduced by a higher-order calculation, as will be the dependence on the renormalization convention of the coupling constants. The line shape in the pole and $\overline{\mathrm{MS}}$ scheme is shown in the left panel of Figure 2.

The effective theory calculation (24) is valid only near resonance when $\sqrt{s}-\hat{M}$ is small, since the expansion inherent to the construction neglects corrections of this order. In other words, near resonance the corrections are of order α or δ, but the second quantity becomes large far off the resonance. To obtain an adequate description of the line shape in the entire kinematical range, the effective theory calculation must be matched to a full theory calculation off resonance. The point to note here is that the full theory calculation of the forward scattering amplitude can be done with ordinary perturbation theory, since no kinematic enhancements invalidate it off resonance. In particular, the optical theorem is applied to intermediate states including the scalar particle as if it were stable.

The off-resonance cross section is only of order α^2 compared to order one near resonance. The result takes the form

$$\sigma = \frac{\pi\alpha_y^2\, s}{(s-\hat{M}^2)^2}\left(f_y(\hat{M}^2/s) + \frac{\alpha_g}{\alpha_y}\,\theta(s-\hat{M}^2)\, f_g(\hat{M}^2/s)\right) \tag{25}$$

with

$$f_y(z) \;=\; 1,$$

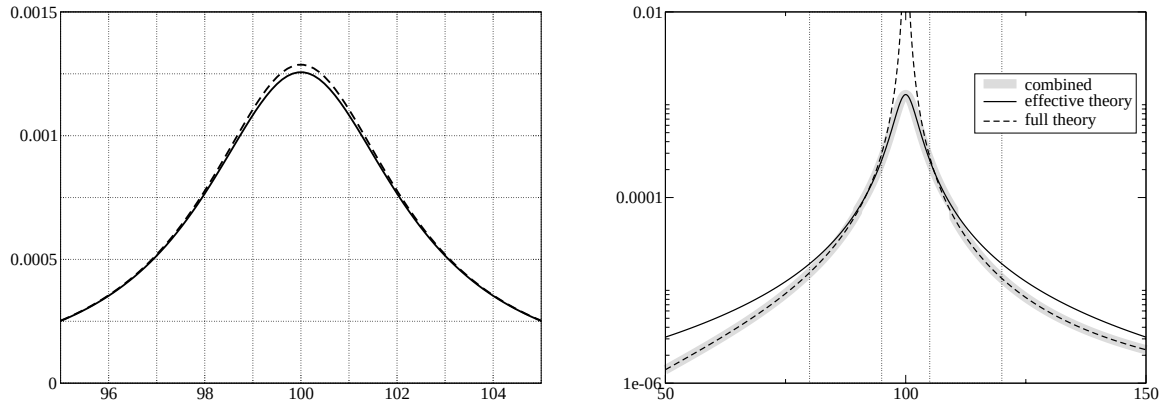

Figure 2: Left panel: line shape (in GeV^{-2}) in the pole (solid) and $\overline{\mathrm{MS}}$ scheme (dashed) as a function of the center-of-mass energy (in GeV). Right panel: Leading-order line shape (in GeV^{-2}) as a function of center-of-mass energy (in GeV) in the effective theory (solid) and the cross section off resonance in the full theory (dashed). The thick grey curve shows the leading-order line-shape with the two curves matched appropriately.

$$f_g(z) \;=\; (1-z)\left\{(1+z^2)\,\ln\frac{s(1-z)^2}{\nu^2} - 2z\right\}. \tag{26}$$

The "partonic" cross section has a collinear divergence, which has been subtracted according to the $\overline{\mathrm{MS}}$ prescription. The physical cross section follows from convoluting the above result with an electron distribution function (in the electron) that depends on the subtraction scale ν. The argument of the logarithm suggests that the collinear factorization scale should be taken to be of order $(s-\hat{M}^2)/\hat{M} \sim \hat{M}\delta$. In the right panel of Figure 2 we show the leading-order computation in the effective theory, and in the full theory off resonance, evaluated at the running scale $\nu = \sqrt{s}\,(1-z)$. The effective theory calculation correctly represents the line shape near the resonance with relative accuracy α. The peak height is of order 1. As the calculation is extrapolated off resonance the cross section decreases and becomes of order α^2. However, in this region the relative error on the effective theory calculation is of order unity. The full theory calculation correctly represents the off-resonance cross section of order α^2 with relative accuracy α. As the calculation is extrapolated towards the resonance, the relative error becomes of order unity. (In fact, the cross section diverges at $s=\hat{M}^2$ and the error becomes arbitrarily large.) The two calculations must be matched in the intermediate region where $\delta \sim (\sqrt{s}-\hat{M})/\hat{M}$ is small enough for both calculations to be valid. The existence of this intermediate region is indicated in the figure by the vertical lines to the left and the right of the resonance peak. We also verify from (24) and (25) that the two calculations agree analytically in this intermediate region. (For completeness we mention that the partonic cross section proportional to $\alpha_y\,\delta(s-\hat{M}^2)$ should be included in the convolution with the electron distribution function, which ensures that

the off-resonance cross section is ν-independent, and sums large logarithms of $\sqrt{s}$ over the electron mass. Since this procedure is standard, we presented the partonic cross section at the running scale, at which no large logarithms occur.)

3 The line shape at next-to-leading order

Following the formalism set up in the previous section we now discuss the matching calculations in more detail. We construct the effective Lagrangian by matching on-shell Green functions and present the explicit form of all terms of the effective Lagrangian that are needed for the evaluation of the line shape at next-to-leading order. At the end of this section we also compute the scattering matrix element in the effective theory to next-to-leading order and obtain the complete NLO line shape.

The matching procedure involves three steps. Compute the renormalized on-shell Green functions in the full theory up to the required order in α. Evaluate the same quantity in the effective theory. Determine the hard matching coefficient so that the two calculations agree within a specified accuracy. The Green functions in the full theory are calculated using conventional weak-coupling perturbation theory. In general, we need an infrared regularization, and the same regularization must be used when computing the corresponding quantity in the effective theory. The result for the matching coefficient is independent of the IR regularization. The calculations become particularly simple with dimensional regularization, since the effective theory loop diagrams vanish in this scheme. This is simply a consequence of the fact that the matching is done on-shell, which renders the corresponding integrals scaleless. However, the matching coefficients depend on a factorization scheme, since the Green functions in the effective theory also exhibit ultraviolet singularities. Thus they have to be UV-subtracted and the choice of the renormalization scheme for the effective theory amounts to the choice of the factorization scheme.

In practice, we simplify the matching procedure by computing directly the hard part of the renormalized on-shell Green functions in the full theory, using the method of regions [11]. This also applies to the Z-factors that multiply the amputated on-shell Green function. Even though the method of regions forces us to use dimensional regularization to define the factorization scheme, we are still free to use another infrared regulator, such as a photon mass, in which case the loop diagrams in the effective theory are generally non-vanishing. However, the result of the hard part is independent of the infrared regularization of the full theory, but it contains infrared $1/\epsilon$ poles due to the separation into hard and soft contributions. These singularities coincide with the above-mentioned UV singularities in the effective theory. We choose to subtract them minimally and thereby define the factorization scheme and the renormalization scheme for the effective theory.

3.1 Matching $\mathcal{L}_{\text{HSET}}$

For the calculation of the line shape at leading order it is sufficient to consider the first term of $\mathcal{L}_{\text{HSET}}$ [Eq. (5)], with the matching coefficient Δ known to order $\alpha \sim \delta$. At next-to-

leading order we will need all terms of order $\{\alpha^2, \alpha\delta, \delta^2\} \times \phi_v^\dagger \phi_v$. Furthermore, at NLO there will also be soft photon loop diagrams in the effective theory, so we will need to include the corresponding terms in the Lagrangian. Since these diagrams will be suppressed by a factor α with respect to the leading-order diagram, the soft photon vertices are only needed at leading order.

3.1.1 The bilinear terms for the unstable field

The bilinear terms of the effective Lagrangian are determined by the dispersion relation for the free-particle states. The field ϕ_v describes a heavy particle near mass-shell, so we need the equivalent of the heavy-quark effective Lagrangian for a scalar field. The only complication is that the scalar is unstable, so the notion of a free-particle state is not really defined. In this case the bilinear terms are constructed so as to reproduce the two-point function near the resonance pole.

In the underlying theory the full renormalized propagator for the unstable particle is given by $i(s - \hat{M}^2 - \Pi(s))^{-1}$, where $-i\,\Pi(s)$ corresponds to the amputated 1PI graphs, including counterterms. Recalling $P = \hat{M}v + k$ the propagator near the resonance pole can be written as

$$\frac{i\,R_\phi}{P^2 - \bar{s}} = \frac{i\,R_\phi}{2\hat{M}vk + k^2 - (\bar{s} - \hat{M}^2)}, \tag{27}$$

where we denoted the complex pole of the propagator by $\bar{s}$ and the residue at the pole by R_ϕ. Defining

$$\Delta \equiv \frac{\bar{s} - \hat{M}^2}{\hat{M}}, \tag{28}$$

we solve $P^2 = \bar{s}$ in the form

$$vk = -\hat{M} + \sqrt{\hat{M}^2 + \hat{M}\Delta - k_\top^2} = \frac{\Delta}{2} - \frac{\Delta^2 + 4k_\top^2}{8\hat{M}} + \mathcal{O}(\delta^3), \tag{29}$$

where for any vector $a_\top^\mu \equiv a^\mu - (va)\,v^\mu$. The second solution has $vk \sim \hat{M}$ and is irrelevant. From this we obtain the effective Lagrangian

$$\mathcal{L}_{\phi\phi} = 2\hat{M}\phi_v^\dagger \left(iv \cdot D_s - \frac{\Delta}{2}\right)\phi_v + 2\hat{M}\phi_v^\dagger \left(\frac{(iD_{s\top})^2}{2\hat{M}} + \frac{\Delta^2}{8\hat{M}}\right)\phi_v + \dots\,. \tag{30}$$

The terms in the second bracket are suppressed by one factor of δ relative to the leading terms. Several comments are in order:

(i) The field ϕ_v is a pure destruction field. Even if the original scalar field had been neutral (real), the corresponding effective scalar field would have been complex, because it contains only the destruction part of the relativistic field. We keep a factor $2\hat{M}$ in the kinetic terms to preserve the canonical mass dimension 1 for a scalar field.

(ii) Since the full Lagrangian is gauge invariant and so is the separation into hard and soft contributions, the effective Lagrangian is also gauge invariant. Therefore, the

interactions of the unstable field with soft photons can be taken into account by replacing ordinary derivatives by covariant derivatives. This has been done in (30).

(iii) The quantity Δ plays the role of a matching coefficient. For a stable particle Δ vanishes in the pole mass scheme and is referred to as "residual mass" in a general scheme. In the unstable case Δ is complex and always non-vanishing. It is Δ that prevents the propagators of the effective theory diagrams from becoming singular. For the interpretation of Δ as a matching coefficient to be consistent, Δ must be given entirely by hard fluctuations. This is related to the fact that the location of the pole of the propagator (27) is infrared-finite. Alternatively, we may note that quantum corrections to the effective theory propagator do not modify the location of the pole to any order in perturbation theory, so the full self-mass must already be contained in the coefficient function Δ. Further, we note that Δ is gauge-independent, because $\bar{s}$ and $\hat{M}$ are gauge-independent.

(iv) Computing the propagator to all orders in δ with the effective Lagrangian (30) does not reproduce (27). Instead we obtain

$$\frac{iR_{\text{eff}\,\phi}}{2\hat{M}\,\left((vP)-\sqrt{\hat{M}^2+\hat{M}\Delta-k_\top^2}\right)} \simeq \frac{i\varpi^{-1}R_{\text{eff}\,\phi}}{P^2-\bar{s}} \tag{31}$$

near the resonance pole, where we used that the coefficients of the higher-order kinetic terms in the effective Lagrangian renormalize in the same way as the leading term due to Lorentz invariance. Besides the different standard residue factors, there also appears the factor

$$\varpi^{-1} \equiv \left(1+\frac{\hat{M}\Delta-k_\top^2}{\hat{M}^2}\right)^{1/2} = 1+\mathcal{O}\left(\alpha,\delta\right), \tag{32}$$

which differs from 1 even at tree level ($\Delta = 0$).

This is due to the fact that (up to the factor $2\hat{M}$) we use the standard form of a non-relativistic Lagrangian, which does not reproduce the normalization of a relativistic field. This is not a problem, because the different normalization is taken into account in matching calculations. Whenever we compute an amputated Green function in the effective theory we multiply every external ϕ_v-line by the additional wave-function normalization factor $\varpi^{-1/2}$. This will be important in Section 3.3, where we discuss the matching of the production (decay) vertex.

3.1.2 Two-loop computation of Δ

The matching coefficient Δ is of order $\hat{M}\delta$ with δ defined in (4) and will be computed from the perturbative expansion of the hard part of the self-energy only. We write the expansion in the form

$$\Pi_h(s) = \hat{M}^2 \sum_{k,l} \delta^l\, \Pi^{(k,l)}, \tag{33}$$

where it is understood that $\Pi^{(k,l)} \sim \alpha^k$. Since the unstable field couples to massless particles the full self-energy is not analytic at $\hat{M}^2$. In particular, for our model $\mathrm{d}\Pi(s)/\mathrm{d}s|_{s=\hat{M}^2}$ has

an infrared singularity. However, only the hard part of the self-energy enters (33). This part is constructed from the Taylor expansion of the Feynman integrand in δ and hence analytic at $\hat{M}^2$, so the Taylor expansion (33) is also well-defined.

The position of the pole of the propagator, $\bar{s}$, and the hard part of the residue at the pole, $R_{h\phi}$, can be expressed in terms of the $\Pi^{(k,l)}$. Up to the third order we find

$$\begin{aligned}\frac{\bar{s}}{\hat{M}^2} &= 1+\Pi^{(1,0)}+\Pi^{(2,0)}+\Pi^{(1,1)}\Pi^{(1,0)} \qquad (34)\\ &\quad +\Pi^{(3,0)}+\Pi^{(2,1)}\Pi^{(1,0)}+\Pi^{(1,1)}\Pi^{(2,0)}+[\Pi^{(1,1)}]^2\Pi^{(1,0)}+\Pi^{(1,2)}[\Pi^{(1,0)}]^2+\ldots.\\ R_{h\phi}^{-1} &= 1-\Pi^{(1,1)}-\Pi^{(2,1)}-2\Pi^{(1,2)}\Pi^{(1,0)} \qquad (35)\\ &\quad -\Pi^{(3,1)}-2\Pi^{(2,2)}\Pi^{(1,0)}-2\Pi^{(1,2)}\Pi^{(2,0)}-2\Pi^{(1,2)}\Pi^{(1,1)}\Pi^{(1,0)}-3\Pi^{(1,3)}[\Pi^{(1,0)}]^2+\ldots.\end{aligned}$$

The first equation allows us to express the matching coefficient Δ [Eq. (28)] in terms of the hard part of the self-energy. Note that even though only the hard part of Π appears in (34), $\bar{s}$ is the physical pole location. In other words, there is no difference whether we use the full self-energy or only its hard part in (34), since Δ receives no soft contributions as discussed above. The situation is different for the residue, since its hard part, as defined in (35), does not in general coincide with the residue of the full propagator R_ϕ that appears in the LSZ reduction formula and in (27). R_ϕ is given by an equation similar to (35) where the hard part is replaced by the full self-energy. The relation reads $R_\phi = R_{h\phi}R_{\text{eff}\,\phi}$. The residues R_ϕ and $R_{\text{eff}\,\phi}$ in the full and effective theory are IR divergent and depend on the IR regulator, but the hard part of the residue is independent of this regularization. However, if dimensional regularization is adopted for the IR singularities, $R_{\text{eff}\,\phi}=1$ (since all loops in the effective theory vanish), and the full and hard residues coincide.

We now turn to the explicit calculation of the matching coefficient

$$\Delta \equiv \sum_i \Delta^{(i)} = \hat{M}\,\Pi^{(1,0)} + \hat{M}\left(\Pi^{(2,0)}+\Pi^{(1,1)}\Pi^{(1,0)}\right)+\ldots \qquad (36)$$

with $\Delta^{(i)}=\mathcal{O}(\alpha^i)$. We need $\Pi^{(1,0)}$ for the calculation of the matching coefficient at leading order, while we need $\Pi^{(2,0)}$ and $\Pi^{(1,1)}$ at NLO. Defining

$$a_g \equiv \frac{\alpha_g}{4\pi}, \quad a_y \equiv \frac{\alpha_y}{4\pi}, \quad a_\lambda \equiv \frac{\lambda}{16\pi^2}, \qquad (37)$$

we find

$$\begin{aligned}\Pi^{(1,0)} &= a_y\left(\frac{\hat{M}^2}{\mu^2}\right)^{-\epsilon}\left(-\frac{2}{\epsilon}-4-8\epsilon+\frac{7\pi^2\,\epsilon}{6}-2i\pi-4i\pi\epsilon\right) \qquad (38)\\ &\quad + a_g\left(\frac{\hat{M}^2}{\mu^2}\right)^{-\epsilon}\left(\frac{3}{\epsilon}+7+15\epsilon+\frac{\pi^2\,\epsilon}{4}\right)+\delta_M^{(1)}-\delta_\phi^{(1)},\\ \Pi^{(1,1)} &= a_y\left(\frac{\hat{M}^2}{\mu^2}\right)^{-\epsilon}\left(-\frac{2}{\epsilon}-2+\frac{7\pi^2\epsilon}{6}-4\epsilon-2i\pi-2i\pi\epsilon\right)-\delta_\phi^{(1)}, \qquad (39)\end{aligned}$$

where $\delta_M^{(1)}$ and $\delta_\phi^{(1)}$ refer to the order α part of the counterterms given in the Appendix. The order ϵ terms will be needed only in (41) below.

The two-loop self-energy has contributions proportional to $\alpha_y\alpha_g$ (4 diagrams), α_y^2 (2 diagrams) and α_g^2 (10 diagrams), not counting counterterm diagrams, as well as a contribution proportional to α_λ, which by assumption is of the same order. The result reads

$$\begin{aligned}
\Pi^{(2,0)} &= \left(\frac{\hat{M}^2}{\mu^2}\right)^{-2\epsilon} a_y a_g \left[-\frac{3}{\epsilon^2}-\frac{17}{2\epsilon}+\frac{17\pi^2}{2}-\frac{99}{4}-24\zeta(3)-\frac{6i\pi}{\epsilon}-39i\pi+\frac{8i\pi^3}{3}\right] \\
&+ \left(\frac{\hat{M}^2}{\mu^2}\right)^{-2\epsilon} a_y^2 \left[-\frac{3}{\epsilon^2}-\frac{5}{2\epsilon}-\frac{11\pi^2}{2}+\frac{57}{4}+\frac{2i\pi}{\epsilon}+5i\pi\right] \\
&+ \left(\frac{\hat{M}^2}{\mu^2}\right)^{-2\epsilon} a_g^2 \left[\frac{8}{\epsilon^2}+\frac{7}{2\epsilon}+\frac{44\pi^2}{3}-\frac{149}{4}+24\zeta(3)-16\pi^2\ln 2\right] \\
&- a_\lambda \left(\frac{\hat{M}^2}{\mu^2}\right)^{-\epsilon} \left(\frac{1}{\epsilon}+1\right) + \Pi_{\rm ct}^{(2)} \qquad (40)
\end{aligned}$$

with the counterterms given by

$$\begin{aligned}
\Pi_{\rm ct}^{(2)} &= \left(\delta_M^{(2)}-\delta_\phi^{(2)}\right) + \left(2\delta_y^{(1)}-\delta_\psi^{(1)}-\delta_\chi^{(1)}\right)\Pi_y^{(1,0)} \\
&+ \left(2\delta_g'^{(1)}-\delta_A^{(1)}-\delta_\phi^{(1)}\right)\Pi_g^{(1,0)} \\
&+ \left(\delta_M^{(1)}-\delta_\phi^{(1)}\right)\hat{M}^2 \frac{\partial\Pi_g^{(1,0)}(\hat{M}^2,P^2)}{\partial\hat{M}^2}\bigg|_{P^2=\hat{M}^2} + \delta_\lambda^{(2)} \int[dk]\,\frac{i}{k^2-\hat{M}^2}. \qquad (41)
\end{aligned}$$

In (41) we indicated the power of α in the counterterms and denoted by $\Pi_y^{(1,0)}$ and $\Pi_g^{(1,0)}$ the contribution to the one-loop self-energy proportional to α_y and α_g respectively, not including counterterms. We adopt the $\overline{\rm MS}$ renormalization scheme and refer to the Appendix for the explicit expressions of the counterterms appearing in (41). The two-loop integrals have been computed with standard techniques. We checked some of our results with recurrence relations from [19], and two-loop master integrals from [20]. Massive one-loop integrals (needed here and later) were in part computed with the method described in [21].

The matching coefficients $\Delta^{(1)}$ and $\Delta^{(2)}$ defined in (36) read in the $\overline{\rm MS}$-scheme

$$\frac{\Delta^{(1)}}{\hat{M}} = a_g\left(-3\ln\frac{\hat{M}^2}{\mu^2}+7\right) + a_y\left(2\ln\frac{\hat{M}^2}{\mu^2}-4-2\,i\pi\right) \qquad (42)$$

$$\begin{aligned}
\frac{\Delta^{(2)}}{\hat{M}} &= a_g^2\left(8\,\ln^2\frac{\hat{M}^2}{\mu^2}+\frac{16}{3}\ln\frac{\hat{M}^2}{\mu^2}-\frac{193}{4}+\frac{40\pi^2}{3}-16\pi^2\log(2)+24\zeta(3)\right) \\
&+ a_y^2\left(\ln^2\frac{\hat{M}^2}{\mu^2}-(11+10\,i\pi)\,\ln\frac{\hat{M}^2}{\mu^2}+\frac{89}{4}-\frac{23\pi^2}{3}+13\,i\pi\right) \\
&+ a_g a_y\left(-9\ln^2\frac{\hat{M}^2}{\mu^2}+(31+12\,i\pi)\ln\frac{\hat{M}^2}{\mu^2}-\frac{115}{4}+5\pi^2-24\zeta(3)-41\,i\pi+\frac{8\,i\pi^3}{3}\right) \\
&+ a_\lambda\left(\ln\frac{\hat{M}^2}{\mu^2}-1\right). \qquad (43)
\end{aligned}$$

We have computed these coefficients in an arbitrary covariant gauge and checked their gauge-parameter independence. Note that $\Pi^{(1,1)}$ and $\Pi^{(2,0)}$ in (39) and (40) have $1/\epsilon$ infrared poles after $\overline{\rm MS}$ renormalization, which must be associated with the factorization of the hard and soft contributions. For $\bar{s}$ and, therefore, for the matching coefficient Δ these singularities cancel as they should. On the other hand, the residue at the pole, R_ϕ, has an infrared singularity in the $\overline{\rm MS}$-scheme. (In the on-shell scheme $R_\phi = 1$ by definition, but in this scheme the field renormalization factor Z_ϕ exhibits the infrared singularity.)

3.1.3 Including soft photons and fermions

To complete the soft Lagrangian $\mathcal{L}_{\rm HSET}$ for the NLO computation the bilinear terms of the unstable field, $\mathcal{L}_{\phi\phi}$, have to be supplemented by the kinetic terms of the soft photon and fermions. Due to gauge invariance, these terms will also contain the interaction terms of a soft photon with a soft charged fermion.

The leading operators scale with δ^4 and are given by the gauge-invariant kinetic terms $\bar{\psi}_s i \not{D}_s \psi_s$, $\bar{\chi}_s i \not{\partial} \chi_s$ and $-1/4\, F_{s\mu\nu} F_s^{\mu\nu}$. By convention the kinetic terms are canonically normalized, and their coefficients do not receive corrections from hard loops. The effective Lagrangian contains an infinite number of higher-dimension operators such as $\bar{\psi}_s \psi_s \bar{\chi}_s \chi_s$ (which scales with δ^6). At NLO we need the operators that scale with δ^5. However, since we assume weak coupling with $g \sim \delta^{1/2}$, at NLO we only need the operators that have non-zero coefficients as $g \to 0$. There are no such operators, so we conclude that at NLO the only relevant soft photon-fermion interaction is contained in $\bar{\psi}_s i \not{D}_s \psi_s$. No further calculation is required to match $\mathcal{L}_{\rm HSET}$ at NLO.

Putting everything together we obtain for $\mathcal{L}_{\rm HSET}$ including all terms needed for the NLO line shape in the weak-coupling limit

$$\begin{aligned}
\mathcal{L}_{\rm HSET} &= 2\hat{M}\phi_v^\dagger \left(iv\cdot D_s - \frac{\Delta^{(1)}}{2} \right) \phi_v + 2\hat{M}\phi_v^\dagger \left(\frac{(iD_{s\top})^2}{2\hat{M}} + \frac{[\Delta^{(1)}]^2}{8\hat{M}} - \frac{\Delta^{(2)}}{2} \right) \phi_v \\
&- \frac{1}{4}\, F_{s\mu\nu} F_s^{\mu\nu} + \bar{\psi}_s i \not{D}_s \psi_s + \bar{\chi}_s i \not{\partial} \chi_s
\end{aligned} \tag{44}$$

with $\Delta^{(1)}$ and $\Delta^{(2)}$ given in (42) and (43) respectively. The first term of (44) gives rise to the unstable particle propagator used in the calculation of the leading-order amplitude (22). All other terms are needed at next-to-leading order only. Note that in writing the Lagrangian (44) we have expanded the matching coefficient Δ in powers of α, so that the unstable particle propagator strictly counts as $1/\delta \sim 1/\alpha$. Alternatively, we could sum higher-order corrections to Δ back into the propagator, although this would not correspond to a strict expansion of the scattering amplitude in δ and α. We will investigate the effect of including additional terms in the propagator in the numerical analysis below.

3.2 Matching $\mathcal{L}_{\rm SCET}$

The leading Lagrangian for the collinear fields has been given in (7). In the position space formulation of soft-collinear effective theory the Lagrangian has been worked out to order

δ in [16]. (We note again that what is called "soft" here has been called "ultrasoft" in [16].) When expanded systematically in powers of $\delta^{1/2}$, the interaction vertices are rather complicated. Our task of writing down all the terms needed for the NLO computation of the line shape is again simplified by the fact that we adopt the weak-coupling limit $g \sim \delta^{1/2}$. Inspection of the expressions in [16] shows that once again there are no relevant operators at order $\delta^{9/2}$ and δ^5 that survive as $g \to 0$. All the vertices needed for collinear loop corrections to the LO line shape are contained in the leading-order Lagrangian

$$\bar{\psi}_c \left(in_- D + i\not{D}_{\perp c} \frac{1}{in_+ D_c + i\epsilon}\, i\not{D}_{\perp c} \right) \frac{\not{n}_+}{2}\, \psi_c. \tag{45}$$

The Feynman rules for the three-point vertices $\bar{\psi}_c \psi_c A_c$ and $\bar{\psi}_c \psi_c A_s$ can be read off from this expression. We may note that the inverse covariant derivative can be written in terms of Wilson lines

$$(in_+ D_c + i\epsilon)^{-1} = W_c\, (in_+ \partial + i\epsilon)^{-1}\, W_c^\dagger, \tag{46}$$

where W_c is

$$W_c(x) = \exp\left(ig \int_{-\infty}^0 ds\, n_+ A_c(x + s n_+) \right). \tag{47}$$

The term (45) therefore contains vertices with any number of A_c fields, which are all leading power in δ, but suppressed by gauge coupling factors g, so they are not needed for the computations of the NLO line shape.

Interactions with soft photons are contained in $\bar{\psi}_c\, in_- D\, \psi_c$. In [16] collinear-soft interaction vertices are light-cone multipole-expanded, and the covariant derivative reduces to $in_- D = in_- \partial + g n_- A_c(x) + g n_- A_{\rm s}(x_-)$ with $x_- = (n_+ x)\, n_-/2$ at leading power. This should be done here only for the coupling of soft fields to the fields describing collinear fluctuations, but not for the coupling to collinear fields with soft fluctuations, since only for the former fields is the transverse momentum large compared to the transverse momentum of soft fields. This affects the way momentum conservation is implemented at the corresponding interaction vertices.

3.3 Production (decay) vertex

The computation of the LO forward scattering amplitude (line shape) requires only the vertex $\phi_v \bar{\psi}_{c1} \chi_{c2}$ + h.c. at tree level. At NLO we therefore need the one-loop coefficient function of this vertex, and production or/and decay vertices suppressed by one factor of δ (without loop corrections).

3.3.1 Power-suppressed vertices

The power-suppressed vertices with field content $\phi_v \bar{\psi}_{c1} \chi_{c2}$ can be obtained to order δ from the result for the heavy-to-light decay current in [16]. However, the result relevant for the forward scattering amplitude can be obtained in a simpler way, since we only wish to reproduce the tree $2 \to 2$ scattering diagram (22) to better accuracy.

For tree-level matching we can set $\Pi(s) = 0$. Leaving out the external spinors and setting $P = \hat{M}v + k$, we obtain by expansion in the small momentum k

$$iy\frac{i}{P^2 - \hat{M}^2}iy^* = iy\frac{i}{2\hat{M}v\cdot k}iy^* + iy\frac{i}{2\hat{M}v\cdot k}ik_\top^2\frac{i}{2\hat{M}v\cdot k}iy^* + i\frac{yy^*}{4\hat{M}^2} + \mathcal{O}(\delta). \tag{48}$$

The first term on the right-hand side is accounted for by the leading-order term in $\mathcal{L}_{\rm HSET}$ together with the leading-order production (decay) vertex. The second term involves one insertion of the kinetic energy correction ($iD_{s\top}^2$) in (44). (For head-on collisions this term vanishes at tree level, because $k_\top = 0$.) The third term is not reproduced by any term in the Lagrangians we discussed so far. Since the intermediate unstable scalar propagator has been canceled by the expansion, we associate this term with the production-decay operator

$$T = \frac{yy^*}{4\hat{M}^2}\,(\bar{\psi}_{c1}\chi_{c2})(\bar{\chi}_{c2}\psi_{c1}). \tag{49}$$

It should be noted that this operator contributes at tree level contrary to the off-shell scattering topologies in the full theory discussed in the previous section. When we distinguish collinear fields with collinear fluctuations from those with soft fluctuations, the operator discussed here appears with field content $(\bar{\psi}_{n_-}\chi_{n_+})(\bar{\chi}_{n_+}\psi_{n_-})$, since each fermion pair describes a configuration with invariant mass close to $\hat{M}^2$. This must be distinguished from the off-shell configurations produced in the scattering of a collinear electron fluctuation off the neutrino. This scattering process is represented at tree-level by a non-local four-fermion operator, but it does not contribute at tree-level to the forward scattering amplitude in the effective theory, resulting in a NNLO contribution.

3.3.2 Hard loop correction

We now turn to the one-loop matching of the coefficient function C of the production (decay) operator

$$J(x) = y\,e^{-i\hat{M}vx}\,[\phi_v\bar{\psi}_{c1}W_{c1}\chi_{c2}](x) + \text{h.c.} \tag{50}$$

Here we have added the Wilson line W_{c1} (see (47)) to the definition of the operator. This generates an infinite number of interaction vertices with additional n_+A_{c1} photons fields, which are not suppressed by powers of δ, but all have the same short-distance coefficient C because of gauge invariance [15]. The Wilson line accounts for full-theory diagrams where a soft ϕ-field emits one or several $c1$-collinear photons and, thereby, becomes off-shell. Integrating out the hard internal ϕ-field results in the Wilson line. At next-to-leading order we are only concerned with the emission of at most one collinear photon, which must then couple to the external electron line attaching to the same production (decay) vertex from which the collinear photon is emitted. We also mention that in principle we should consider the emission of photons collinear with the neutrino from the electron or the heavy scalar, which puts the electron or scalar lines off-shell. However, the effect cancels due to the charge-neutrality of the neutrino. It is for this reason that we do not introduce a $c2$-collinear photon field in the effective theory.

We begin the one-loop computation of C by specifying the matching prescription. In the underlying theory we compute the amputated, $\overline{\rm MS}$-renormalized, on-shell three-point function of an electron, neutrino and scalar field, multiplied by the LSZ residue factors, and expand it to leading order in δ. The corresponding three-point function in the effective theory contains one insertion of the operator $y\, e^{-i\hat{M}vx}\,[\phi_v \bar{\psi}_{c1} W_{c1}\chi_{c2}](x)$. Denoting this three-point function by $\Gamma_{\rm eff}$ and the former by Γ, the matching equation reads

$$\sqrt{R_\psi}\sqrt{R_\chi}\sqrt{R_\phi}\,\Gamma = C\,\varpi^{-1/2}\sqrt{R_{{\rm eff}\,\psi}}\sqrt{R_{{\rm eff}\,\chi}}\sqrt{R_{{\rm eff}\,\phi}}\,\Gamma_{\rm eff} \tag{51}$$

Here the various R-factors denote the ultraviolet-finite LSZ residues in the $\overline{\rm MS}$ scheme given by the ratios of the on-shell and $\overline{\rm MS}$ field renormalization constants. The factor $\varpi^{-1/2}$ defined in (32) appears because of the non-relativistic normalization of the field ϕ_v. Its origin can be understood most directly by comparing the scalar propagators in full and effective theory diagrams as done in (31). Note that the on-shell condition for the scalar line implies that its momentum satisfies $P^2 = \bar{s} = \hat{M}^2 + \hat{M}\Delta$, but in a perturbative matching calculation this condition must be fulfilled only to the appropriate order in α and δ. For the one-loop matching of C it is sufficient to put $P^2 = \hat{M}^2$.

The matching equation (51) is valid for any infrared regulator, but becomes particularly simple in the case of dimensional regularization, where all loop diagrams in the effective theory vanish on-shell. Then all the effective theory residues equal 1, $\Gamma_{\rm eff}$ equals its tree-level value and the matching equation becomes

$$\sqrt{R_{h\psi}}\sqrt{R_{h\chi}}\sqrt{R_{h\phi}}\sqrt{\varpi}\;\Gamma_h = C\,\Gamma_{\rm tree} \tag{52}$$

The full theory quantities must then be equal to their hard contribution in the sense of the expansion by regions, and since ϖ can be expressed in terms of the short-distance coefficient Δ, this equation says that we can obtain C by directly computing the hard contributions in the full theory.

The residue $R_{h\phi}$ can be obtained from (35) and (39), and the residues $R_{h\psi}$ and $R_{h\chi}$ can be computed in a similar way. The results are given in the Appendix. There is only one one-loop diagram and one counterterm diagram contributing to Γ at next-to-leading order. Evaluating the hard part of this one-loop diagram we obtain

$$\Gamma_h = iy\left(1 + a_g\left(\frac{\hat{M}^2}{\mu^2}\right)^{-\epsilon}\left(-\frac{1}{\epsilon^2} - \frac{1}{\epsilon} - 2 - \frac{\pi^2}{12}\right) + \delta_y^{(1)}\right) \tag{53}$$

We can now apply (52) to find the matching coefficient at NLO. Together with

$$\varpi = 1 - \frac{\Delta^{(1)}}{2\hat{M}} + \mathcal{O}\left(\alpha^2, \alpha\delta, \delta^2\right) \tag{54}$$

and the residues from the Appendix we obtain $C = 1 + C^{(1)} + \mathcal{O}\left(\alpha^2\right)$, where

$$\begin{aligned} C^{(1)} &= a_y\left[\log\frac{\hat{M}^2}{\mu^2} - \frac{1}{4} - \frac{i\pi}{2}\right] \\ &+ a_g\left[-\frac{1}{\epsilon^2} + \frac{1}{\epsilon}\left(\ln\frac{\hat{M}^2}{\mu^2} - \frac{5}{2}\right) - \frac{1}{2}\ln^2\frac{\hat{M}^2}{\mu^2} + \frac{7}{4}\ln\frac{\hat{M}^2}{\mu^2} - \frac{15}{4} - \frac{\pi^2}{12}\right]. \end{aligned} \tag{55}$$

Figure 3: Hard contributions to the next-to-leading order amplitude. Left: Insertion of $[\Delta^{(1)}]^2/4$ and $-\hat{M}\Delta^{(2)}$. Right: Insertion of $C^{(1)}$, the symmetric diagram is understood.

The poles are infrared poles related to the factorization of hard and soft contributions. The final result for $C^{(1)}$ is obtained by subtracting the pole part. (In the following $C^{(1)}$ refers to this subtracted expression.) It is independent of the gauge parameter ξ as it should be, because the production (decay) operator is gauge-invariant. The double logarithm in the coefficient of a_g is related to the infrared divergence in Γ_h. The single logarithms on the other hand are also related to the scale dependence of the Yukawa coupling y.

3.4 Forward scattering amplitude in the effective theory

We are now in the position to compute the forward scattering amplitude at next-to-leading order in the effective theory.

The first class of contributions consists of diagrams with the topology of the tree diagram (22), but with corrections to the propagator and the production (decay) vertex as shown in Figure 3. As can be seen from (44), the relevant terms for the left diagram of Figure 3 are $[\Delta^{(1)}]^2/4$ and $-\hat{M}\Delta^{(2)}$. The remaining term $(iD_{s\top})^2$ does not lead to a contribution at NLO. First for head-on collisions the scalar line has $k_\top = 0$. Secondly, the photon vertices from this term contribute only at NNLO for weak coupling g. The other diagrams in this class are obtained from the hard corrections to the Wilson coefficient C of the production (decay) vertex. (The production and decay operator have the same complex coefficient C, and not the complex conjugates to each other, see (50).) There are two such diagrams, one of which is displayed in Figure 3. Adding up these three diagrams we obtain

$$i\,\mathcal{T}_h^{(1)} = i\,\mathcal{T}^{(0)} \;\times\; \left[2\,C^{(1)} - \frac{[\Delta^{(1)}]^2}{8\mathcal{D}\hat{M}} + \frac{\Delta^{(2)}}{2\mathcal{D}}\right] \tag{56}$$

with

$$\mathcal{D} \equiv \sqrt{s} - \hat{M} - \frac{\Delta^{(1)}}{2}. \tag{57}$$

All these diagrams correspond to corrections due to hard loops and, thus, can be identified with the factorizable corrections [10]. These corrections are separately gauge invariant since so are the matching coefficients. In addition there is the contribution from the

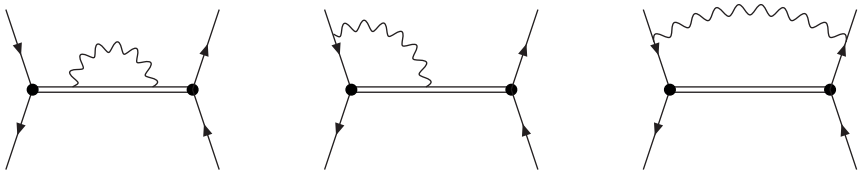

Figure 4: Soft contributions to the next-to-leading order amplitude. A diagram with a soft correction at the decay vertex is understood.

production-decay operator T in (49), which contributes to $i\,\mathcal{T}_h^{(1)}$ the term

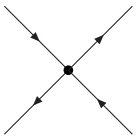

$$= \frac{iyy^*s}{8\hat{M}^2} = i\,\mathcal{T}^{(0)} \times \left[-\frac{\mathcal{D}}{2\hat{M}}\right]. \tag{58}$$

We now turn to the one-loop corrections in the effective theory, which are due to soft or collinear photons. The loop provides a factor of α, so at NLO in a combined expansion in α and δ we can use the leading power soft and collinear photon vertices. We begin with the soft correction. The coupling of the soft photon to the ϕ_v-field is given by the covariant derivative in the first term in $\mathcal{L}_{\rm HSET}$ (44), whereas the coupling to the collinear electron can be obtained from the first term in $\mathcal{L}_{\rm SCET}$ (7). With dimensional infrared regularization the residue factors equal 1, which leaves the diagrams shown in Figure 4. For the forward scattering amplitude the box diagram (third diagram in Figure 4) vanishes in Feynman gauge, because the photon-coupling to the collinear electron is proportional to n_-^μ. Thus the amplitude is proportional to $n_-^2 = 0$. Computing the remaining diagrams of Figure 4 we obtain

$$i\,\mathcal{T}_s^{(1)} = i\,\mathcal{T}^{(0)} \;\times\; a_g \left(\frac{-2\mathcal{D}}{\mu}\right)^{-2\epsilon} \left[\frac{2}{\epsilon^2} + \frac{2}{\epsilon} + 4 + \frac{5\pi^2}{6}\right]. \tag{59}$$

The final result for the soft amplitude is the above expression with the pole terms subtracted after expanding the prefactor $(-2\mathcal{D}/\mu)^{-2\epsilon}$. The soft part of the amplitude does not contain logarithms of the hard scale as expected. We also note that the soft amplitude is gauge-invariant, because it is computed with a gauge-invariant effective Lagrangian.

The only collinear photon correction at NLO comes from the diagram shown in Figure 5 (and the corresponding symmetric diagram), where the collinear photon coupling at the production (decay) vertex is derived from the Wilson line in (50). However, for an on-shell electron the integral is scaleless and vanishes in dimensional regularization.

Combining (56), (58), (59) with the result for the matching coefficient $C^{(1)}$ in (55) we obtain for the forward scattering amplitude at next-to-leading order

$$i\,\mathcal{T}^{(1)} = i\,\mathcal{T}^{(0)} \quad \times \quad \left[\, a_g \left(3 + 4\,\log\frac{-2\hat{M}\mathcal{D}}{\hat{M}^2}\right)\left(-\frac{1}{\epsilon} + \log\frac{-2\hat{M}\mathcal{D}}{\mu^2}\right)\right.$$

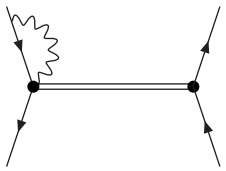

Figure 5: Contributions to the next-to-leading order amplitude involving collinear photons.

$$+\, a_g \left(-7 \log \frac{-2\hat{M}\mathcal{D}}{\hat{M}^2} - \frac{3}{2} \log \frac{\hat{M}^2}{\mu^2} - \frac{7}{2} + \frac{2\pi^2}{3} \right)$$
$$+\, a_y \left(2 \log \frac{\hat{M}^2}{\mu^2} - \frac{1}{2} - i\pi \right) - \frac{[\Delta^{(1)}]^2}{8\mathcal{D}\hat{M}} + \frac{\Delta^{(2)}}{2\mathcal{D}} - \frac{\mathcal{D}}{2\hat{M}} \Bigg]. \qquad (60)$$

Rather than inserting the subtracted expressions for $\mathcal{T}_s^{(1)}$ and $C^{(1)}$ we have used here the unsubtracted ones to display the structure of singularities. The double poles in $1/\epsilon$ have canceled between the hard and soft corrections, but there are $1/\epsilon$ poles left over from $\mathcal{T}^{(1)}$, which must be associated with the collinear singularity due to initial state radiation from the massless electron. To verify that these singularities have the expected structure we compute

$$[i\,\mathcal{T}_{\rm sing}^{(1)}/s] = -\frac{\alpha_g}{2\pi} \int_0^1 dx\, \frac{1}{\epsilon}\, P(x)\, [i\,\mathcal{T}^{(0)}(xs)/(xs)] \qquad (61)$$

where $i\,\mathcal{T}^{(0)}(xs)$ is the leading-order forward scattering amplitude given in (22), but with s replaced by xs. (x is the momentum fraction of the electron in the electron.) Furthermore

$$P(x) = \frac{2}{[1-x]_+} + \frac{3}{2}\,\delta(1-x) \qquad (62)$$

is the soft limit of the $e \to e$ Altarelli-Parisi splitting function, and we took into account that the incoming neutrino does not radiate photons. Simplifying the splitting function to the soft limit is justified, because values of x not near one correspond to hard-collinear radiation, and this is a NNLO effect (which is part of the production-decay operator in the right panel of Figure 1). Similarly the x-integral could be restricted to an interval close to one. Equivalently, we perform the x-integration from zero to one and expand the result around $\sqrt{s} = \hat{M}$ to obtain

$$i\,\mathcal{T}_{\rm sing}^{(1)} = i\,\mathcal{T}^{(0)} \times \left(-\frac{a_g}{\epsilon} \right) \left(3 + 4 \log \frac{-2\hat{M}\mathcal{D}}{\hat{M}^2} \right), \qquad (63)$$

which agrees with the pole part of (60). This confirms that the cross section is finite once the initial-state singularities have been factored into the electron distribution function.

Subtracting the initial-state singularities minimally according to our convention for the electron distribution function, we obtain

$$
\begin{aligned}
i\,\mathcal{T}^{(1)} = i\,\mathcal{T}^{(0)} \quad \times \quad \Bigg[\; a_g \Bigg(& 3 \log \frac{-2\hat{M}\mathcal{D}}{\nu^2} + 4 \, \log \frac{-2\hat{M}\mathcal{D}}{\hat{M}^2} \log \frac{-2\hat{M}\mathcal{D}}{\nu^2} \\
& - 7 \log \frac{-2\hat{M}\mathcal{D}}{\hat{M}^2} - \frac{3}{2} \log \frac{\hat{M}^2}{\mu^2} - \frac{7}{2} + \frac{2\pi^2}{3} \Bigg) \\
& + a_y \left(2 \log \frac{\hat{M}^2}{\mu^2} - \frac{1}{2} - i\pi \right) - \frac{[\Delta^{(1)}]^2}{8\mathcal{D}\hat{M}} + \frac{\Delta^{(2)}}{2\mathcal{D}} - \frac{\mathcal{D}}{2\hat{M}} \; \Bigg]
\end{aligned}
\tag{64}
$$

as the final result for the next-to-leading order contribution to the forward scattering amplitude. The correction to the inclusive line shape is given by the imaginary part of this expression. We have introduced the scale ν to distinguish the scale of the electron distribution function from the renormalization scale in the masses and couplings. Referring to (25) we note that ν should be taken of order $\hat{M}\delta$ to make the initial-state collinear logarithms small.

We performed several further checks of this result. First we find that the logarithms of μ cancel the scale dependence of $\hat{M}$ and yy^* in $i\,\mathcal{T}^{(0)}$ to NLO. Second we expand $1/s \times \mathrm{Im}\,(\mathcal{T}^{(0)} + \mathcal{T}^{(1)})$ to order α^2 and compare this to the expansion of the fixed-order cross section (25) to order α^2/δ. The two expansions coincide in the terms α^2/δ^2, α^2/δ, which they have in common. Finally, we have also computed the δ expansion of the one-loop forward scattering amplitude directly in the full theory. This checks all the terms in (64) except for those involving $\Delta^{(2)}$ and $[\Delta^{(1)}]^2$, which come from two-loop diagrams in the full theory.

The final result (64) is given in the $\overline{\rm MS}$ scheme. We briefly discuss how to translate this result to the pole renormalization scheme, where the mass M is defined by $\bar{s} = M^2 - iM\Gamma$ and the residue of the renormalized ϕ-propagator is $R_\phi = 1$. All other renormalization conventions remain unchanged. From the definition of Δ in (28) we obtain in the pole scheme $\mathrm{Re}\,\Delta_p = 0$ and

$$
\mathrm{Im}\,\frac{\Delta_p}{M} = \frac{\mathrm{Im}\,(\Delta/\hat{M})}{1 + \mathrm{Re}\,(\Delta/\hat{M})}
\tag{65}
$$

with Δ and $\hat{M}$ referring to the $\overline{\rm MS}$ (or, in fact, any other) scheme. Using (42), (43) we obtain

$$
\frac{\Delta_p^{(1)}}{M} = -2\,i\pi a_y,
\tag{66}
$$

$$
\frac{\Delta_p^{(2)}}{M} = i\pi a_y^2 \left(-6 \ln \frac{M^2}{\mu^2} + 5 \right) + i\pi a_g a_y \left(6 \ln \frac{M^2}{\mu^2} - 27 + \frac{8\pi^2}{3} \right).
\tag{67}
$$

To convert the matching coefficient C to the pole scheme, we observe that $R_\phi Z_\phi$ is scheme-independent, so the only modification comes from the normalization factor ϖ, resulting in

$$
C_p = \left(\frac{\varpi_p}{\varpi} \right)^{1/2} C, \qquad 2C_p^{(1)} = 2C^{(1)} + \frac{\mathrm{Re}\,\Delta^{(1)}}{2\hat{M}}.
\tag{68}
$$

This is exactly what is needed to render the line shape scheme-independent to leading order in δ and to all orders in α. Using (65) and (68) together with $M^2 = \hat{M}^2 + \hat{M}\,\mathrm{Re}\,\Delta$ we find $C_p^2/M = C^2/\hat{M}$, so

$$\frac{C_p^2}{M\Big(\sqrt{s} - \sqrt{M^2 + M\Delta_p}\Big)} = \frac{C^2}{\hat{M}\Big(\sqrt{s} - \sqrt{\hat{M}^2 + \hat{M}\Delta}\Big)} \tag{69}$$

exactly.

3.5 Next-to-leading order line shape

We compute the line shape at NLO in the $\overline{\mathrm{MS}}$ renormalization scheme by taking the imaginary part of $(\mathcal{T}^{(0)} + \mathcal{T}^{(1)})/s$. The result depends on the renormalization scale μ and rather strongly on the collinear factorization scale ν. This dependence would be canceled (up to the order at which we perform the calculation), if we folded our cross section with the electron distribution function. Since this is well understood and we are interested in displaying the next-to-leading order effects intrinsic to the line-shape calculation, we present the partonic cross section, and adopt $\mu = M$ and $\nu = |2\mathcal{D}|$ unless otherwise stated, since this choice makes the collinear logarithms unimportant.

In order to illustrate the numerics we use $a_g = 0.1/(4\pi)$, $a_y = 0.1/(4\pi)$ and $a_\lambda = (0.1)^2/(4\pi)^2$ and assume the pole mass $M = 100$ GeV. For the plots in the $\overline{\mathrm{MS}}$ scheme we have to convert the pole mass to the $\overline{\mathrm{MS}}$ mass $\hat{M}$. At LO we use the one-loop relation between the pole mass and $\hat{M}$ and obtain $\hat{M} = 98.8$ GeV, whereas at NLO we use the two-loop relation and get $\hat{M} = 99.1$ GeV. The LO line shape has already been shown in Figure 2. In Figure 6 (upper panel) we show the LO and the NLO line shape in the $\overline{\mathrm{MS}}$ scheme (solid curves) and the pole scheme (dashed curves). The scheme dependence is very small, but the next-to-leading order correction is around -10% near the peak, and can be up to -30% for center-of-mass energies between 95 GeV and 105 GeV . The ratio of NLO to LO is shown as the solid line in the lower panel of the figure.

Contrary to the LO line-shape the NLO line shape does not any longer have an exact (non-relativistic) Breit-Wigner shape. Performing a fit of the NLO line shape ($\overline{\mathrm{MS}}$ scheme) to a Breit-Wigner curve in the range $95 \le \sqrt{s} \le 105$ GeV we find deviations up to 15%. The ratio of the NLO curve to the Breit-Wigner fit is shown in as dashed line in Figure 6. Moreover, the output mass parameter of the Breit-Wigner fit differs from the input $M = 100\,\mathrm{GeV}$ by $-160\,\mathrm{MeV}$. This illustrates that in realistic situations the data should be fitted to the theoretically predicted shape rather than a Breit-Wigner-type ansatz.

Up to now we have performed a strict expansion in the couplings and δ to obtain the NLO result. In particular, we only included $\Delta^{(1)}$ in the propagator and treated the terms $\Delta^{(2)}$ as well as higher powers of $\Delta^{(1)}$ as interactions in a perturbative expansion. In other words, we used $i/(2\hat{M}\mathcal{D})$ for the propagator of the unstable field. A slightly different approach is to include the effect of higher-order bilinear terms in the Lagrangian into the propagator, which sums these terms to all orders. This can be done in different versions.

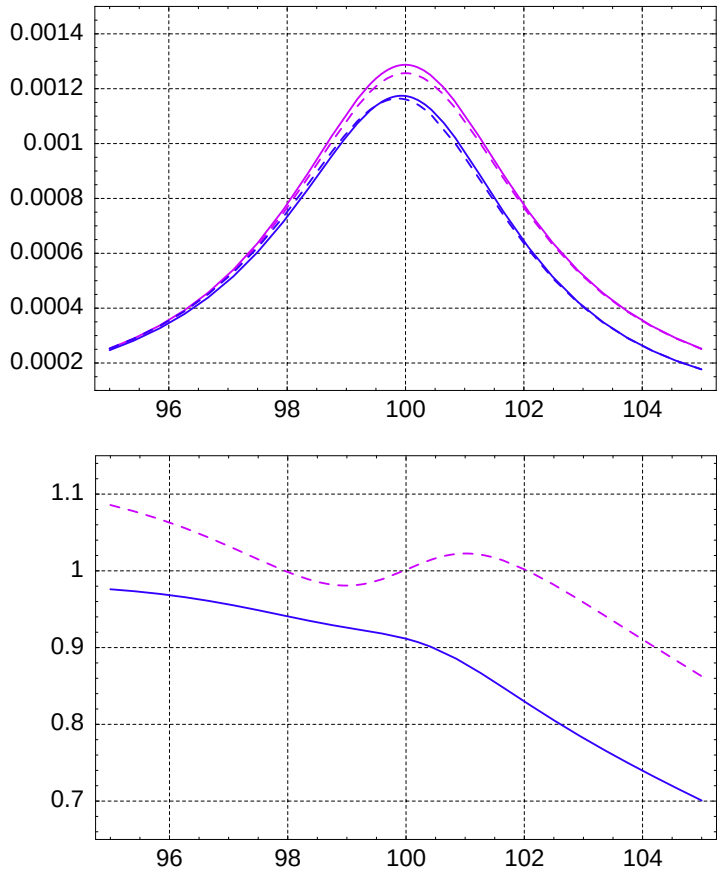

Figure 6: Upper panel: line shape (in GeV^{-2}) in the $\overline{\mathrm{MS}}$ scheme (solid) and pole scheme (dashed) at LO (upper magenta/light grey curves) and NLO (lower blue/dark grey curves) as a function of the center-of-mass energy in GeV. Lower panel: The ratio of the NLO to the LO line shape in the $\overline{\mathrm{MS}}$ scheme (solid blue/dark grey curve) and the ratio of the NLO $\overline{\mathrm{MS}}$ line shape to a Breit-Wigner fit (dashed magenta/light grey curve).

For example, instead of $\Delta^{(1)}$ we may use the full Δ. At NLO, this implies using the propagator

$$\frac{i}{2\hat{M}(\mathcal{D}-\Delta^{(2)}/2)} \tag{70}$$

which absorbs the interaction term $\Delta^{(2)}/2\mathcal{D}$ and sums all powers of $\Delta^{(2)}$ in the forward scattering amplitude. The difference to the non-summed line shape is of course a NNLO effect. The ratio of summed to non-summed line shape at NLO is shown as the dashed curves in Figure 7 in the $\overline{\mathrm{MS}}$ scheme (blue/dark grey line) and the pole scheme (magenta/light grey line). In computing the resummed line shape we have adapted the factorization scale and used $\nu = |2\mathcal{D} - \Delta^{(2)}|$. It can be seen from Figure 7 that the effect of resummation

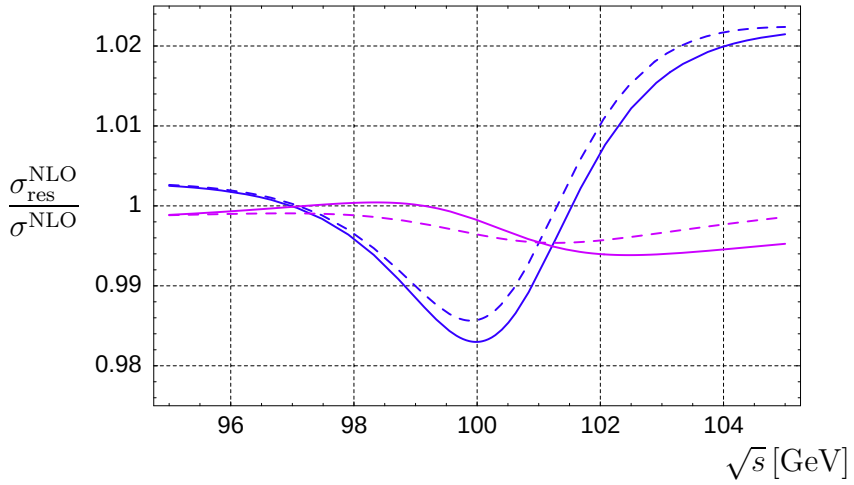

Figure 7: The ratio of the line shape with powers of $\Delta^{(2)}$ (and $\Delta^{(1)}$) resummed over the non-summed line shape in the pole (magenta/light grey lines) and $\overline{\rm MS}$ scheme (blue/dark grey lines). The dashed curves represent the line shape including $\Delta^{(2)}$ in the propagator. Resumming also all powers of $\Delta^{(1)}$ results in the solid curves.

is less than 2%, which indicates that the higher-order terms associated with $\Delta^{(2)}$ are not large. The effect is still smaller in the pole scheme.

We can go one step further and also resum all terms associated with the expansion of Δ. In order to achieve this we have to recall that we obtained the propagator by expanding $vk = -\hat{M} + \sqrt{\hat{M}^2 + \hat{M}\Delta - k_\top^2}$ in Δ and $k_\top$ (see (29)). Expanding only $k_\top^2$ we obtain the summed propagator, which at NLO reads

$$\frac{i}{2\hat{M}(\sqrt{s} - \sqrt{\hat{M}^2 + \hat{M}(\Delta^{(1)} + \Delta^{(2)})})}. \tag{71}$$

This also absorbs the interaction term $-[\Delta^{(1)}]^2/8M\mathcal{D}$ into the propagator. The ratio of corresponding summed to non-summed line shape at NLO is shown as the solid curves in Figure 7 in the $\overline{\rm MS}$ scheme (blue/dark grey line) and the pole scheme (magenta/light grey line). (The factorization scale has been adapted to $\nu = 2|(\sqrt{s} - \sqrt{M^2 + M(\Delta^{(1)} + \Delta^{(2)})})|$.) Again the effect of resummation is marginal compared to the size of the NLO correction.

4 Beyond NLO

A crucial aspect of our formalism is that it allows to improve the accuracy of the calculations by including systematically higher-order corrections. After the explicit calculation of the line shape at NLO, we now discuss how to go beyond NLO. We will outline the necessary calculations to obtain the line shape at NNLO in the effective theory approach. Then we compute explicitly a subset of corrections to illustrate once more how the formalism automatically maintains gauge invariance of the calculation.

4.1 Elements of the NNLO calculation

Since we perform a double expansion in α and δ, the NNLO computation must include all terms suppressed with respect to the LO result by either α^2, δ^2 or $\alpha\delta$. In order to facilitate the classification of terms we also distinguish between radiative corrections due to hard (h), collinear (c), and soft (s) loops, denoting the coupling α with the corresponding subscript. For example, a two-loop matrix element correction in the effective theory with no further suppression by δ will be denoted as α_s^2, if both loops are soft, and if the vertices do not include hard corrections. With this in mind we proceed to the discussion of various NNLO contributions.

1) Tree amplitude in the effective theory with insertions of LO operators in δ, matched to NNLO (α_h^2)

The effective theory diagrams are the same as in Figure 3, but now the propagator and hard vertex corrections must be included to higher accuracy in α. This implies the computation of $\Delta^{(3)}$, which, from (28) and (34), can be seen to involve $\Pi^{(3,0)}$, the three-loop self-energy at $P^2 = \hat{M}^2$, as the most difficult part. In addition, the two-loop hard correction $C^{(2)}$ to the production (decay) vertex $\phi_v \bar{\psi}_{c1}\chi_{c2}$ is required. These are standard loop calculations, which are difficult, but not impossible with present Feynman diagram technologies. Both matching coefficients, $\Delta^{(3)}$ and $C^{(2)}$, are gauge invariant.

2) Tree amplitude in the effective theory with insertions of NLO operators in δ, matched to NLO ($\alpha_h\delta$)

The number of possible terms of this type is limited by the requirement that they contribute to the tree $2 \to 2$ scattering amplitude in the effective theory. NLO operators can be constructed from the LO operators by acting on soft and collinear fields with extra derivatives. The Wilson coefficients of these operators then have to be matched up to NLO. Operators with bilinear terms in the fields require no work, since they are determined by the dispersion relation for the free field. Operators generated by adding derivatives to the LO production (decay) operator can be eliminated by the equation of motions or do not contribute at tree level for external states with vanishing transverse momentum.

This leaves genuine NLO operators. An example is the four-fermion production-decay operator (49),

$$\frac{yy^*}{4\hat{M}^2}\,(\bar{\psi}_{c1}\chi_{c2})(\bar{\chi}_{c2}\psi_{c1}),$$

that we encountered already in the computation of the NLO scattering amplitude. At NNLO we therefore need the hard radiative correction to the coefficient function. The corresponding calculation is done explicitly in the subsequent subsection. In general, production (decay) operators need not be local. Consider a collinear electron fluctuation with momentum $\hat{M}n_-/2 + k_1$ (where n_+k_1 is of order $\hat{M}$ for a collinear fluctuation) scattering on the neutrino with momentum $\hat{M}n_+/2 + k_2$, where k_2 is small. In this case, the scalar

propagator is $i/(\hat{M}n_+k_1)$, which is far off-shell but does not correspond to a local interaction vertex. However, as discussed before, these non-local operators do not have tree matrix elements with the external collinear modes in $2 \to 2$ scattering.

Finally, there is a one-loop correction to the four-fermion production-decay operator that arises indirectly. Loop corrections induce an effective soft photon-neutrino coupling

$$\frac{g a_y}{\hat{M}^2} \left(\bar{\chi}_{c2} \gamma_\nu \chi_{c2}\right) \partial_\mu F_s^{\mu\nu} \tag{72}$$

Although this operator scales as $g\alpha_y\delta^4$, which is $g\alpha_y\delta^2$ suppressed relative to the neutrino kinetic term, it contributes to the NNLO forward scattering amplitude through soft-photon exchange in the t-channel, because the soft photon propagator cancels the δ^2 suppression. This can be seen directly by converting (72) to the four-fermion operator using the soft photon equation of motion. In the following subsection we compute the coefficient function and discuss how this operator contributes to the tree scattering amplitude in the effective theory. There exists also a similar electron-photon coupling. However, in this case there is no tree scattering diagram due to the absence of a tree-level neutrino-photon coupling.

3) Tree amplitude in the effective theory with insertions of NNLO operators in δ, matched to LO (δ^2)

The task of writing down all relevant δ^2 suppressed operators is simplified by the fact that we do not consider further suppressions by α. Hence we only need to expand the tree $2 \to 2$ scattering diagram in the underlying theory one order further than in (48). We then find the NNLO production (decay) vertex $\bar{\psi}_{c1}\chi_{c2}(iD_{s\top})^2\phi_v$ (which in fact gives no contribution in the center-of-mass frame of the collision, where $k_\top = 0$), and the NNLO production-decay operator

$$-\frac{y y^*}{8\hat{M}^3} \left(\bar{\psi}_{c1}\chi_{c2}\right) ivD_s \left(\bar{\chi}_{c2}\psi_{c1}\right), \tag{73}$$

which produces a correction proportional to $(\sqrt{s} - \hat{M})/\hat{M}^3$ to the line shape.

4) One-loop amplitude in the effective theory with insertions of LO operators in δ, matched to NLO ($\alpha_s\alpha_h, \alpha_c\alpha_h$)

The one-loop scattering diagrams are those shown in Figure 4, however, now there is an additional insertion of $[\Delta^{(1)}]^2/4$ or $-\hat{M}\Delta^{(2)}$ into the scalar propagator, or the production (decay) vertex is taken at NLO, involving the correction $C^{(1)}$, similar to the tree diagrams in Figure 3. These terms can be obtained from the calculation in the previous section without further work. We simply multiply (59) by C^2, interpret $\mathcal{D}$ as $\sqrt{s} - (\hat{M}^2 + \hat{M}(\Delta^{(1)} + \Delta^{(2)}))^{1/2}$, expand in α and δ and pick out the NNLO terms. Note that in the underlying theory the two-loop diagrams corresponding to these contributions involve soft and hard loops, hence in the conventional terminology these are neither purely factorizable nor purely non-factorizable corrections. Nevertheless, the effective theory formalism guarantees that

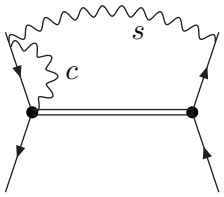

Figure 8: Contribution to the next-to-next-to-leading order amplitude involving collinear (and soft) photons.

this set of terms is gauge-independent. Since the collinear one-loop contribution shown in Figure 5 vanishes, it follows that there are no terms proportional to $\alpha_c\alpha_h$.

5) One-loop amplitude in the effective theory with insertions of NLO operators in δ, matched to LO ($\alpha_s\delta, \alpha_c\delta$)

We have already discussed possible NLO operators in the category *2)*, but some of the simplifications based on the properties of the external momenta of the tree amplitude in the effective theory no longer apply to the one-loop amplitude. For instance, the residual momentum $k_\top$ of the internal scalar line no longer vanishes, and a non-zero contribution from the insertion of $(iD_{s\top})^2$ into the scalar propagator is obtained. In principle one may also need new production (decay) operators with collinear or soft photon fields in addition to the basic structure $\phi_v\bar{\psi}_{c1}\chi_{c2}$. The problem of deriving the operators at tree-level is very similar to deriving the power-suppressed heavy-to-light decay current in soft-collinear effective theory [16]. Since the collinear one-loop diagrams vanish, the interesting operators are those with a soft photon field, but it turns out that after applying the field equations, there is no gauge-invariant operator of this sort. It follows that the set of possible NNLO terms is again rather limited. One $\alpha_s\delta$ term that appears is the soft one-loop correction to the local four-fermion interaction shown in (58).

6) Two-loop amplitude in the effective theory with insertions of LO operators in δ, matched to LO ($\alpha_s^2, \alpha_s\alpha_c, \alpha_c^2$)

The final set of terms involves a two-loop calculation of the forward scattering amplitude in the effective theory, including vertex- and box-type corrections. However, since the propagators and vertices of the leading-order effective Lagrangian are much simpler than those in the underlying theory, the two-loop calculation is also greatly simplified. It is worth noting that in this calculation there appear for the first time non-vanishing collinear loop integrals. A representative diagram is shown in Figure 8. The requirement is that the external electron first emits a soft photon, so that the subsequent collinear emission occurs from an off-shell line. The collinear loop integral is then no longer scaleless. Because of this requirement, however, there are no contributions where both loops are collinear.

This concludes the classification of terms. It is evident that a NNLO calculation of the line shape can be performed in the effective field theory approach without conceptual difficulties. In fact, the previous discussion shows that the most difficult calculations are reduced to standard calculations of a hard two-loop vertex correction and the on-shell three-loop self-energy. In particular, the difficulty of maintaining gauge invariance is absent in this approach. Since the separation of terms by momentum scales is gauge-independent, the sum of all contributions with a given power of δ, α_h, α_c, and α_s is separately gauge-independent.

In the version of the effective theory where collinear fluctuations are integrated out, the collinear loop contributions move from the effective theory matrix element to a matching correction. The calculations to be performed remain of course the same, but the structure of operators is different, since the effective theory no longer contains fields for collinear fluctuations. While this simplifies the field content of possible operators, it also complicates their structure, introducing new non-localities related to the fact that one component of collinear momentum is of the same order as the soft momentum. There is again a close analogy with recent developments in soft-collinear effective theory, which, however, we do not pursue further here.

4.2 One-loop matching of the production-decay operator

In this subsection we perform an explicit calculation of the $\alpha_h\delta$ contributions to the forward scattering amplitude categorized under *2)* above.

4.2.1 Four-fermion operator

The four-fermion operator (49) is a sub-leading operator that gives rise to a production-decay vertex. It contributes to the forward scattering amplitude at NLO through the tree diagram (58). We now determine the loop correction to the coefficient function of this vertex.

Consider the box diagram contribution to the scattering amplitude in the full theory shown in Figure 9. It is clear that the hard part of this diagram results in a loop correction to a local four-fermion operator. This contribution alone is gauge-dependent. However, there are additional contributions from vertex and self-energy corrections (also shown in Figure 9), since expanding the corresponding subgraphs in δ results in terms where the propagators of the unstable scalar are canceled. Because of this cancellation these terms also contribute to the coefficient of the local four-fermion operator, rendering the complete result gauge-independent.

To see this, consider first the terms proportional to $\alpha_y\alpha_g$ in Figure 9. Due to the two scalar propagators, the leading contribution from the self-energy diagram is of order α^2/δ^2. This is a LO contribution, which is already included in the effective theory through the propagator $i/(2\hat{M}(vk) - \hat{M}\Delta^{(1)})$ of the scalar field. The next term in the expansion in δ cancels one propagator, resulting in a local vertex. This is already included in the computation of the matching coefficient $C^{(1)}$. The second term in the expansion in δ,

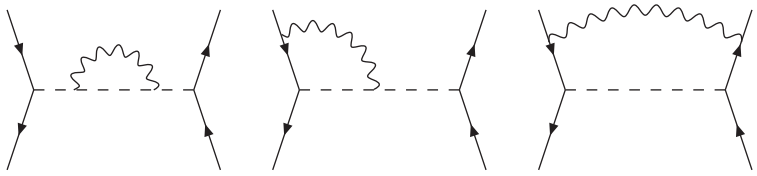

Figure 9: Diagrams in the full theory proportional to $\alpha_y \alpha_g$, whose hard part contributes to the matching coefficient of the production-decay vertex at NLO. A diagram with a vertex correction at the decay vertex is understood.

however, results in a NNLO contribution, which has to be reproduced by the effective theory via the matching coefficient of the production-decay vertex. Similarly, the leading contribution from the vertex diagram is included in $C^{(1)}$, and we need the next term in the expansion in δ, where the scalar propagator is canceled. We then obtain for the contribution from the self-energy, vertex and box diagrams

$$\begin{aligned}
B_{\rm se}^{(2)} &= i|y|^2 \frac{[\bar{u}(p)v(q)]\,[\bar{v}(q)u(p)]}{\hat{M}^2}\,\Pi^{(1,2)} \\
&= \frac{i|y|^2 a_g}{\hat{M}^2}[\bar{u}(p)v(q)]\,[\bar{v}(q)u(p)]\,\left(-\frac{3-\xi}{2\,\epsilon}+\frac{3-\xi}{2}\ln\frac{\hat{M}^2}{\mu^2}+(1-\xi)\right), \qquad (74) \\
B_{\rm v}^{(2)} &= \frac{i|y|^2 a_g}{\hat{M}^2}[\bar{u}(p)v(q)]\,[\bar{v}(q)u(p)]\,\left(-\frac{2}{\epsilon^2}+\frac{2-\xi}{\epsilon}+\frac{2}{\epsilon}\ln\frac{\hat{M}^2}{\mu^2}\right. \\
&\quad \left.-(2-\xi)\ln\frac{\hat{M}^2}{\mu^2}-\ln^2\frac{\hat{M}^2}{\mu^2}-2(4-\xi)-\frac{\pi^2}{6}\right), \qquad (75) \\
B_{\rm b}^{(2)} &= \frac{i|y|^2 a_g}{\hat{M}^2}[\bar{u}(p)v(q)]\,[\bar{v}(q)u(p)]\,\left(-\frac{1-\xi}{2\epsilon}+\frac{1-\xi}{2}\ln\frac{\hat{M}^2}{\mu^2}+(1-\xi)\right) \\
&+ \frac{i|y|^2 a_g}{\hat{M}^2}[\bar{u}(p)\gamma^\mu\gamma^\nu v(q)]\,[\bar{v}(q)\gamma_\nu\gamma_\mu u(p)]\,\left(-\frac{1}{2\epsilon}+\frac{1}{2}\ln\frac{\hat{M}^2}{\mu^2}-\frac{3}{2}\right). \qquad (76)
\end{aligned}$$

Summing (74), (75) and (76) we see that the gauge dependence cancels, and we obtain

$$\frac{iB_1}{\hat{M}^2}[\bar{u}(p)v(q)]\,[\bar{v}(q)u(p)]+\frac{iB_2}{\hat{M}^2}[\bar{u}(p)\gamma^\mu\gamma^\nu v(q)]\,[\bar{v}(q)\gamma_\nu\gamma_\mu u(p)] \qquad (77)$$

with

$$\begin{aligned}
B_1 &= -|y|^2 a_g\left(\frac{2}{\epsilon^2}-\frac{2}{\epsilon}\ln\frac{\hat{M}^2}{\mu^2}+\ln^2\frac{\hat{M}^2}{\mu^2}+6+\frac{\pi^2}{6}\right), \\
B_2 &= -|y|^2 a_g\left(\frac{1}{2\epsilon}-\frac{1}{2}\ln\frac{\hat{M}^2}{\mu^2}+\frac{3}{2}\right). \qquad (78)
\end{aligned}$$

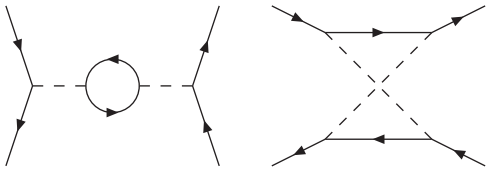

Figure 10: Diagrams in the full theory proportional to α_y^2, whose hard part contributes to the matching coefficient of the production-decay vertex at NLO.

The cancellation of the gauge dependence is of course not accidental. Since the separation of hard and soft parts is gauge-invariant, and since we match S-matrix elements, the short-distance coefficient must be gauge-independent.

There are further contributions to the matching coefficient. First, the terms proportional to α_y^2 from the diagrams shown in Figure 10 are given by

$$\frac{iB_3}{\hat{M}^2}[\bar{u}(p)v(q)]\,[\bar{v}(q)u(p)] + \frac{iB_4}{\hat{M}^2}[\bar{u}(p)\not{q}u(p)]\,[\bar{v}(q)\not{p}v(q)] + \frac{iB_5}{\hat{M}^2}[\bar{u}(p)\gamma^\mu u(p)]\,[\bar{v}(q)\gamma_\mu v(q)] \quad (79)$$

with

$$B_3 = -|y|^2 a_y, \qquad B_4 = -|y|^2 a_y\left(-5+\frac{\pi^2}{2}\right), \qquad B_5 = -|y|^2 a_y\left(1-\frac{\pi^2}{12}\right). \quad (80)$$

Second, up to now we have been discussing contributions which (with the exception of the box diagrams) come from expanding the one-particle irreducible self-energy or vertex subgraphs in δ. Additional contributions arise from the expansion of the one-particle reducible scalar propagator according to (48). For instance, combining the local NLO term from (48) with the (renormalized) hard vertex at leading order in δ, we obtain a contribution to the coefficient of the four-fermion operator proportional to $C^{(1)}$. Similar terms come from the self-energy diagram. Collecting all contributions, we obtain for the NLO correction to the production-decay operator (49)

$$\begin{aligned}
T^{(1)} \;=\; & -\frac{|y|^2}{\hat{M}^2}\,(\bar{\psi}_{c1}\chi_{c2})(\bar{\chi}_{c2}\psi_{c1})\Bigg[a_y + a_g\left(\frac{2}{\epsilon^2}-\frac{2}{\epsilon}\ln\frac{\hat{M}^2}{\mu^2}+\ln^2\frac{\hat{M}^2}{\mu^2}+\frac{\pi^2}{6}+6\right) \\
& \qquad -\frac{C^{(1)}}{2}+\frac{\Delta^{(1)}}{16\hat{M}}\Bigg] \\
& -\frac{|y|^2}{\hat{M}^2}\,(\bar{\psi}_{c1}\gamma_\nu\gamma_\mu\chi_{c2})\,(\bar{\chi}_{c2}\gamma^\mu\gamma^\nu\psi_{c1})\;a_g\left(\frac{1}{2\epsilon}-\frac{1}{2}\ln\frac{\hat{M}^2}{\mu^2}+\frac{3}{2}\right) \\
& -\frac{|y|^2}{\hat{M}^2}\left(\bar{\psi}_{c1}\frac{\not{n}_+}{2}\psi_{c1}\right)\left(\bar{\chi}_{c2}\frac{\not{n}_-}{2}\chi_{c2}\right)a_y\left(-5+\frac{\pi^2}{2}\right) \\
& -\frac{|y|^2}{\hat{M}^2}\,(\bar{\psi}_{c1}\gamma^\mu\psi_{c1})\,(\bar{\chi}_{c2}\gamma_\mu\chi_{c2})\;a_y\left(1-\frac{\pi^2}{12}\right), \qquad (81)
\end{aligned}$$

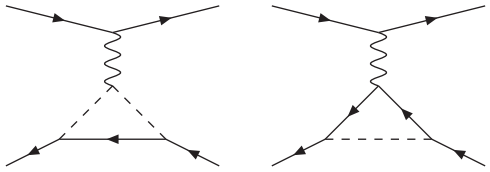

Figure 11: NNLO forward scattering diagrams in the full theory with a soft photon exchanged in the t-channel. The hard contribution to the triangle subgraph generates the effective photon-neutrino coupling $(\bar{\chi}\chi)\partial F$.

with $\Delta^{(1)}/\hat{M}$ and $C^{(1)}$ given in (42) and (55), respectively. Inserting the explicit expressions for these quantities, the poles in ϵ do not cancel. The left-over poles are related to the factorization of hard, collinear and soft contributions, and the initial-state collinear singularity, and are canceled only once all other NNLO contributions to the scattering amplitude are combined. The final result for the matching coefficient is obtained from the above expression with all poles subtracted minimally.

We expressed (81) in terms of four-fermion operators with four Dirac structures as they come out of the calculation. Not all of them are independent. Using Fierz transformations and the projection properties $\not{n}_-\psi_{c1} = \not{n}_+\chi_{c2} = 0$ of the collinear fermion fields, they can be reduced to linear combinations of the three basis operators

$$(\bar{\psi}_{c1}\chi_{c2})(\bar{\chi}_{c2}\psi_{c1}), \qquad (\bar{\psi}_{c1}\gamma_5\chi_{c2})(\bar{\chi}_{c2}\gamma_5\psi_{c1}), \qquad (\bar{\psi}_{c1}\gamma_{\mu_\perp}\chi_{c2})(\bar{\chi}_{c2}\gamma^{\mu_\perp}\psi_{c1}), \tag{82}$$

where "$\mu_\perp$" means that one sums only over the transverse components. To perform this reduction, it is necessary to define carefully the Dirac algebra in d dimensions in very much the same way as in applications of the weak effective Hamiltonian to weak interaction processes at low energies.

4.2.2 Effective photon-neutrino coupling

There is a second correction of order $\alpha_h\delta$, which we discuss separately, although it can be interpreted as a further contribution to (81). Consider the two diagrams in the full theory displayed in Figure 11, which do not involve resonant scalar lines. The hard contribution to the triangle subgraphs (consisting of scalar and electron lines) induces an effective soft-photon neutrino coupling. The result of the calculation gives

$$\frac{g a_y}{\hat{M}^2}\,(\bar{\chi}_{c2}\gamma_\nu\chi_{c2})\,\partial_\mu F_s^{\mu\nu}\left[\frac{1}{3\epsilon} - \frac{1}{3}\ln\frac{\hat{M}^2}{\mu^2} + \frac{1}{2}\right]. \tag{83}$$

In Figure 11 the photon must be soft, because we consider the forward scattering amplitude. (In fact, to regulate the otherwise divergent t-channel propagator, we must temporarily consider the amplitude slightly non-forward.) Power counting shows that this is a δ^2 suppressed operator. The factor of δ^2 is compensated by the t-channel photon propagator

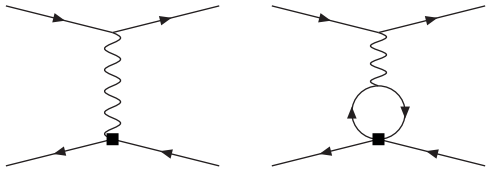

Figure 12: Effective theory tree diagrams related to the full theory diagrams in Figure 11. The left-hand diagram involves the $(\bar{\chi}\chi)\partial F$ coupling, the right-hand diagram the mixed collinear-soft four-fermion operator and a soft electron loop.

of order $1/\delta^2$, the result being an $\alpha_g\alpha_y$ (NNLO) contribution to the scattering amplitude in the effective theory shown as the left-hand diagram of Figure 12. The photon propagator is canceled by a momentum factor from the vertex (83) resulting in a local contribution to the scattering amplitude of the same form as (81). This can be seen explicitly using the soft photon equation of motion $\partial_\mu F_s^{\mu\nu} = -g\,\bar{\psi}_{c1}\gamma^\nu\psi_{c1} + \ldots$ to rewrite (83) as a four-fermion operator times a coefficient proportional to $|y|^2 a_g$.

The $1/\epsilon$ pole in (83) is a soft divergence, which arises due to the hard-soft factorization from the second diagram in Figure 11. The divergence cancels with the soft contribution to this diagram, where the two internal electron lines are soft, and the scalar line is off-shell. The off-shell scalar induces a local $(\bar{\chi}_{c2}\psi_s)(\bar{\psi}_s\chi_{c2})$ vertex. This mixed collinear-soft four-fermion operator contributes to the forward scattering amplitude in the effective theory through the one-loop diagram shown on the right-hand side of Figure 12, where the electron loop is soft. Once again the δ^2 suppression of the operator is compensated by the soft photon propagator.

5 Summary and outlook

It has been recognized for some time that the perturbative treatment of unstable particles is difficult, because partial summations of the perturbative expansion are necessary. These difficulties originated mainly from the fact that the guiding principle for resummation was not understood. In this paper we advocated the idea that effective field theory methods familiar from other applications in high-energy physics can be adapted to solve the problem of describing systematically the production and decay of unstable particles, since the fundamental reason for the breakdown of weak-coupling perturbation theory is related to the emergence of a second (small) momentum scale near resonance. The advantages of the effective theory method are:

- It breaks the calculation into several well-defined pieces (matching calculations, matrix element calculations), thus rendering the organization of the calculation efficient and transparent.

- It provides a power-counting scheme in the small parameters (δ, couplings), which

allows for an identification of the terms relevant for achieving a prescribed accuracy before actual calculations must be done.

- It provides a set of (Feynman) rules to compute the minimal set of terms necessary for a given accuracy. Since one does not calculate "too much", the calculation to a given order is presumably technically simpler than in any other approach.

- Gauge invariance is automatic at every order, since the effective Lagrangian is gauge-invariant.

- It can be extended to any accuracy in the expansion in δ and in couplings at the expense of performing more complicated, but well-defined calculations.

In this paper we explained these ideas in a toy theory restricting ourselves to a single scalar resonance, an abelian gauge theory, and a totally inclusive resonant scattering cross section. Extending the method to non-abelian gauge theories or relaxing any of the other restrictions causes only technical complications. For instance, for a resonant fermion, the heavy scalar Lagrangian would be replaced by the familiar heavy quark effective Lagrangian. For resonant gauge bosons in the electroweak Standard Model in R_ξ gauge with ξ not near one, the degrees of freedom with mass $\xi\hat{M}^2$ are integrated out, and the effective theory contains a massive vector field with three polarizations. Non-renormalizability is not an issue, since the effective field describes only soft fluctuations. In 't Hooft-Feynman gauge, or with ξ close to one, the effective theory contains a vector field with four polarizations and a pseudo-Goldstone field, which cancels the effect of the scalar polarization state, so that one can work again with a canonical massive vector field.

Other obvious extensions of this work concern non-inclusive kinematics and pair production of unstable particles. In these cases it will be necessary to enlarge the field content of the effective theory. For instance, if energetic particles (jets) are detected in the final state, one must introduce new collinear fields corresponding to the direction of these particles. It is advantageous to work with cut diagrams rather than amplitudes, so that the (final-state weighted) phase-space integrals can be treated on the same footing as loop diagrams in matching calculations. Similarly the extension to pair production requires the introduction of two copies of what we called the HSET Lagrangian in this paper, one for each unstable particle with different velocity vectors. The production (decay) vertices then depend on additional kinematic quantities such as the scalar product of the velocities. Pair production near threshold appears in this context as the particular case, where the two velocities become nearly equal. The two HSET Lagrangian then merge to the non-relativistic Lagrangian, and standard methods can be applied to deal with the potential complications due to the strong Coulomb force. We are confident that effective field theory will be the method of choice to address unstable particle production in these different kinematic situations and plan to return to some of them in the context of concrete applications.

Acknowledgements

We thank M. Kalmykov for correspondence. The work of M.B. and A.C. is supported by the DFG Sonderforschungsbereich/Transregio 9 "Computer-gestützte Theoretische Teilchenphysik". We also acknowledge the use of the Mathematica packages FeynCalc and FeynArts [22] for performing some of the loop calculations.

Appendix

In this appendix we collect the renormalization factors and counterterms of the theory defined by the Lagrangian (2). The counterterm Lagrangian is

$$\begin{aligned}\mathcal{L}_{\rm ct} &= \delta_\phi\,\partial_\mu\phi^\dagger\partial^\mu\phi - \delta_M\hat{M}^2\phi^\dagger\phi + \delta_\psi\bar{\psi}i\partial\!\!\!/\psi + \delta_\chi\bar{\chi}i\partial\!\!\!/\chi - \frac{\delta_A}{4}F^{\mu\nu}F_{\mu\nu} \\ &\quad + \delta_g g\mu^\epsilon\bar{\psi}A\!\!\!/\psi + \delta'_g g\mu^\epsilon\left(\phi^\dagger A_\mu i\partial^\mu\phi - (i\partial^\mu\phi^\dagger)A_\mu\phi\right) + \delta_{g^2}g^2\mu^{2\epsilon}\phi^\dagger A_\mu A^\mu\phi \\ &\quad + \delta_y y\mu^\epsilon\phi\bar{\psi}\chi + \delta_y^* y^*\mu^\epsilon\phi^\dagger\bar{\chi}\psi - \frac{\delta_\lambda}{4}\mu^{2\epsilon}(\phi^\dagger\phi)^2. \end{aligned} \tag{84}$$

The relation between bare and renormalized quantities is

$$\begin{array}{ll} \phi_0 = \sqrt{Z_\phi}\phi, & \delta_\phi = Z_\phi - 1, \\ M_0^2 = Z_M^2\hat{M}^2, & \delta_M = Z_M^2 Z_\phi - 1, \\ \psi_0 = \sqrt{Z_\psi}\psi, & \delta_\psi = Z_\psi - 1, \\ \chi_0 = \sqrt{Z_\chi}\chi, & \delta_\chi = Z_\chi - 1, \\ A_0 = \sqrt{Z_A}A, & \delta_A = Z_A - 1, \\ \xi_0 = Z_A\xi, & \\ g_0 = Z_g g\mu^\epsilon, & \delta_g = Z_g Z_\psi\sqrt{Z_A} - 1, \\ y_0 = Z_y y\mu^\epsilon, & \delta_y = Z_y\sqrt{Z_\phi}\sqrt{Z_\psi}\sqrt{Z_\chi} - 1, \\ \lambda_0 = (\lambda+\Delta_\lambda)\mu^{2\epsilon} & \delta_\lambda = (Z_\phi^2 - 1)\lambda + Z_\phi^2\Delta_\lambda, \end{array} \tag{85}$$

The counterterms δ'_g and δ_{g^2} are not independent, but determined by the previous ones:

$$\begin{aligned} \delta'_g &= Z_g Z_\phi\sqrt{Z_A} - 1, \\ \delta'_{g^2} &= Z_g^2 Z_\phi Z_A - 1. \end{aligned} \tag{86}$$

In this paper all renormalization constants are needed at the one-loop order except for Z_M^2, which must be known to two loops. In the $\overline{\rm MS}$ scheme, and in covariant gauge with gauge parameter ξ, the counterterms expressed in terms of the renormalized couplings are given by:

$$Z_y = 1 + \frac{1}{\epsilon}\left(-\frac{3}{2}\,a_g + \frac{3}{2}\,a_y\right)$$

$$
\begin{aligned}
Z_g &= 1+\frac{1}{\epsilon}\left(\frac{5}{6}\,a_g\right)\\
Z_\phi &= 1+\frac{1}{\epsilon}\left((3-\xi)\,a_g-2\,a_y\right)\\
Z_\psi &= 1+\frac{1}{\epsilon}\left(-\xi a_g-\frac{1}{2}\,a_y\right)\\
Z_\chi &= 1+\frac{1}{\epsilon}\left(-\frac{1}{2}\,a_y\right)\\
Z_A &= 1+\frac{1}{\epsilon}\left(-\frac{5}{3}\,a_g\right)\\
Z_M^2 &= 1+\frac{1}{\epsilon}\left(-3\,a_g+2\,a_y\right)+\frac{1}{\epsilon^2}\left(8\,a_g^2+a_y^2-9\,a_g a_y\right)\\
&\quad+\frac{1}{\epsilon}\left(\frac{53}{6}\,a_g^2-\frac{3}{2}\,a_y^2+\frac{5}{2}\,a_g a_y+a_\lambda\right)
\end{aligned}
\tag{87}
$$

Furthermore, we need the part of δ_λ that is proportional to α_y^2 and α_g^2. It is given by

$$
\delta_\lambda=-\frac{8\,\alpha_y^2}{\epsilon}+\frac{12\,\alpha_g^2}{\epsilon}. \tag{88}
$$

The ultraviolet-finite residues of the $\overline{\rm MS}$-renormalized propagators read:

$$
\begin{aligned}
R_\phi &= 1-(3-\xi)\,\frac{1}{\epsilon}a_g+a_y\left(2\log\frac{\hat{M}^2}{\mu^2}-2-2\,i\pi\right)\\
R_\psi &= 1+\frac{\xi}{\epsilon}a_g+a_y\left(\frac{1}{2}\log\frac{\hat{M}^2}{\mu^2}-\frac{1}{4}\right)\\
R_\chi &= 1+a_y\left(\frac{1}{2}\log\frac{\hat{M}^2}{\mu^2}-\frac{1}{4}\right)\\
R_A &= 1+a_g\left(\frac{1}{3}\log\frac{\hat{M}^2}{\mu^2}+\frac{4}{3\epsilon}\right)
\end{aligned}
\tag{89}
$$

The $1/\epsilon$ poles in these equations are infrared divergences. In the dimensional infrared regularization scheme the full residues equal their hard contributions, so $R_{hX}=R_X$.

References

[1] D. Y. Bardin *et al.*, "Electroweak working group report", in *Reports of the working group on precision calculations for the Z resonance*, Eds. D. Bardin, W. Hollik and G. Passarino, (CERN-95-03, Genève, 1995), [hep-ph/9709229].

[2] W. Beenakker, F. A. Berends and A. P. Chapovsky, Nucl. Phys. B **548** (1999) 3 [hep-ph/9811481];
A. Denner, S. Dittmaier, M. Roth and D. Wackeroth, Phys. Lett. B **475** (2000) 127 [hep-ph/9912261];
A. Denner, S. Dittmaier, M. Roth and D. Wackeroth, Nucl. Phys. B **587** (2000) 67 [hep-ph/0006307];
S. Jadach *et al.*, Phys. Rev. D **61** (2000) 113010 [hep-ph/9907436].

[3] W. Beenakker, F. A. Berends and A. P. Chapovsky, Phys. Lett. B **454** (1999) 129 [hep-ph/9902304];
N. Kauer and D. Zeppenfeld, Phys. Rev. D **65** (2002) 014021 [hep-ph/0107181];
M. L. Nekrasov, Phys. Lett. B **545** (2002) 119 [hep-ph/0207215].

[4] E. N. Argyres *et al.*, Phys. Lett. B **358** (1995) 339 [hep-ph/9507216];
W. Beenakker *et al.*, Nucl. Phys. B **500** (1997) 255 [hep-ph/9612260];
G. Passarino, Nucl. Phys. B **574** (2000) 451 [hep-ph/9911482].

[5] W. Beenakker, F. A. Berends and A. P. Chapovsky, Nucl. Phys. B **573** (2000) 503 [hep-ph/9909472];
W. Beenakker *et al.*, [hep-ph/0303105].

[6] R. G. Stuart, Phys. Lett. B **262** (1991) 113;
A. Aeppli, G. J. van Oldenborgh and D. Wyler, Nucl. Phys. B **428** (1994) 126 [hep-ph/9312212].

[7] V. S. Fadin, V. A. Khoze and A. D. Martin, Phys. Rev. D **49** (1994) 2247;
K. Melnikov and O. I. Yakovlev, Phys. Lett. B **324** (1994) 217 [hep-ph/9302311].

[8] K. Melnikov and O. I. Yakovlev, Nucl. Phys. B **471** (1996) 90 [hep-ph/9501358];
W. Beenakker, A. P. Chapovsky and F. A. Berends, Nucl. Phys. B **508** (1997) 17 [hep-ph/9707326]; Phys. Lett. B **411** (1997) 203 [hep-ph/9706339];
A. Denner, S. Dittmaier and M. Roth, Nucl. Phys. B **519** (1998) 39 [hep-ph/9710521]; Phys. Lett. B **429** (1998) 145 [hep-ph/9803306].

[9] F. V. Tkachov, [hep-ph/9802307];
F. V. Tkachov, [hep-ph/0001220];
M. L. Nekrasov, Eur. Phys. J. C **19** (2001) 441 [hep-ph/0002184].

[10] A. P. Chapovsky, V. A. Khoze, A. Signer and W. J. Stirling, Nucl. Phys. B **621** (2002) 257 [hep-ph/0108190].

[11] M. Beneke and V. A. Smirnov, Nucl. Phys. **B522** (1998) 321 [hep-ph/9711391];
V. A. Smirnov, *Applied Asymptotic Expansions In Momenta And Masses*, Springer Verlag, Berlin, Germany, 2002.

[12] M. Beneke, A.P. Chapovsky, A. Signer and G. Zanderighi, [hep-ph/0312331].

[13] E. Eichten and B. Hill, Phys. Lett. **B234** (1990) 511;
H. Georgi, Phys. Lett. **B240** (1990) 447;
B. Grinstein, Nucl. Phys. **B339** (1990) 253.

[14] C. W. Bauer, S. Fleming and M. E. Luke, Phys. Rev. D **63** (2001) 014006 [hep-ph/0005275].

[15] C. W. Bauer, S. Fleming, D. Pirjol, and I. W. Stewart, Phys. Rev. **D63** (2001) 114020 [hep-ph/0011336];
C. W. Bauer, D. Pirjol, and I. W. Stewart, Phys. Rev. **D65** (2002) 054022 [hep-ph/0109045].

[16] M. Beneke, A. P. Chapovsky, M. Diehl and Th. Feldmann, Nucl. Phys. B **643** (2002) 431 [hep-ph/0206152];
M. Beneke and Th. Feldmann, Phys. Lett. B **553** (2003) 267 [hep-ph/0211358].

[17] M. J. Dugan and B. Grinstein, Phys. Lett. B **255** (1991) 583.

[18] M. J. Veltman, Physica **29** (1963) 186.

[19] O. V. Tarasov, Nucl. Phys. B **502** (1997) 455 [hep-ph/9703319];
R. Mertig and R. Scharf, Comput. Phys. Commun. **111** (1998) 265 [hep-ph/9801383].

[20] J. Fleischer, M. Y. Kalmykov and A. V. Kotikov, Phys. Lett. B **462** (1999) 169 [hep-ph/9905249];
J. Fleischer, M. Y. Kalmykov and A. V. Kotikov, [hep-ph/9905379];
J. Fleischer and M. Y. Kalmykov, Comput. Phys. Commun. **128** (2000) 531 [hep-ph/9907431].

[21] A. I. Davydychev, J. Math. Phys. **32** (1991) 1052;
E. E. Boos and A. I. Davydychev, Theor. Math. Phys. **89** (1991) 1052 [Teor. Mat. Fiz. **89** (1991) 56].

[22] R. Mertig, M. Böhm and A. Denner, Comput. Phys. Commun. **64** (1991) 345;
J. Kublbeck, M. Böhm and A. Denner, Comput. Phys. Commun. **60** (1990) 165.